Am J Cancer Res 2022;12(4):1707-1726
www.ajcr.us /ISSN:2156-6976/ajcr0142252

Original Article

E2F1-mediated GINS2 transcriptional activation promotes tumor progression through PI3K/AKT/mTOR pathway in hepatocellular carcinoma

Yao Zhang[1*], Xiaopei Hao[1*], Guoyong Han[1*], Yiwei Lu[1*], Zhiqiang Chen[1], Long Zhang[1], Jindao Wu[1,2], Xuehao Wang[1]

[1]*Hepatobiliary Center, The First Affiliated Hospital of Nanjing Medical University, Key Laboratory of Liver Transplantation, Chinese Academy of Medical Sciences, Nanjing 210029, Jiangsu, China;* [2]*State Key Laboratory of Reproductive Medicine, Nanjing Medical University, Nanjing, Jiangsu, China.* [*]*Equal contributors.*

Received February 9, 2022; Accepted March 23, 2022; Epub April 15, 2022; Published April 30, 2022

Abstract: Hepatocellular carcinoma (HCC) has high morbidity and mortality rates. It is therefore imperative to study the underlying mechanism of HCC to identify potential prognostic biomarkers and therapeutic targets. Recently, GINS2 has been identified to be a cancer-promoting gene in different cancer types. Nevertheless, the exact mechanism of GINS2 in HCC remains to be elucidated. To systematically explore the significance of GINS2, we first assessed the relative expression of GINS2 in pan-cancers based on data obtained from the HCCDB, TIMER, and TCGA databases. Then, we explored the clinical significance of GINS2 in HCC through Kaplan-Meier method as well as univariate and multivariate cox regression analysis. Additionally, functional enrichment analysis of GINS2 was done through GO, KEGG, PPI network, and immune cell infiltration analyses. Functional experiments were also conducted to investigate the biological significance of GINS2 in HCC cell lines. Our research revealed that GINS2 is involved in HCC progression and highlighted its potential value as a crucial diagnostic and therapeutic target for HCC.

Keywords: Hepatocellular carcinoma, E2F1, GINS2, PI3K/AKT/mTOR

Introduction

Hepatocellular carcinoma (HCC) is a morphologically heterogeneous cancer type with several histologic subtypes and different structural growth patterns [1]. Due to the high prevalence of hepatitis B, the incidence rate of HCC has been rising in China [2]. Most HCC cases are diagnosed at advanced stages that lack curative therapies and have low resectability rates [3-5]. Meanwhile, the development of new therapies for advanced HCC has been hampered by an insufficient understanding of the underlying molecular mechanisms [6]. As a result, it is critical to identify possible genes and signaling pathways that regulate the progression of HCC.

The GINS complex (GINS) consists of PSF1, PSF2, PSF3, and SLD5 [7, 8], and maintains DNA replication forks by interacting with the MCM2-MCM7 complex [9]. It is involved in regulating cell cycle as well as cell proliferation and apoptosis [10]. GINS complex subunit 2 (GINS2, also named PSF2), encoded by the *GINS2* gene, is located on human chromosome 16q24 [11]. Previous studies have indicated aberrant expression of GINS2 in multiple tumors. For example, the overexpression of GINS2 promotes EMT via activating the ERK/MAPK signal pathway in pancreatic cancer [12]. Upregulated GINS2 promotes tumor progression in NSCLC [13]. And knockdown of GINS2 inhibits cell proliferation in human gliomas [14]. It has also been shown that GINS2 is upregulated in HCC tumor tissues, suggesting the potential of GINS2 as a therapeutic target [15-17]. Nevertheless, how GINS2 functions in the progression of HCC is still unclear. We describe in this report our investigation of the role of GINS2 in HCC progression and strive to shed light on its underlying mechanism.

Materials and methods

PPI network construction and functional annotation analysis

The PPI (protein-protein interaction) network of GINS2-related proteins was constructed through GeneMANIA database (http://genemania.org/). Gene ontology analysis (GO) has broad applications in the functional annotation of large-scale genomic data. The KEGG database contains information about biological pathways. GO and KEGG analyses were completed with the Cluster Profiler in R package.

Analysis of tumor-infiltrating immune cells

The tumor-infiltrating immune cell analysis was performed using TIMER2.0 (https://cistrome.shinyapps.io/timer/). Additionally, single sample Gene Enrichment Analysis (ssGSEA) was used in the determination of correlation between GINS2 and 24 subtypes of immune cells using the R package.

HCCDB database analysis

We examined the mRNA expression level of GINS2 through the HCCDB database (http://lifeome.net/database/hccdb), which consists of 15 datasets and nearly 4,000 clinical samples from the TCGA database and Gene Expression Omnibus (GEO) [18].

Kaplan-Meier survival curve analysis

The OS (overall survival), PFS (progression-free survival), DSS (disease-free survival), and RFS (recurrence-free survival) curves of HCC patients were obtained from the Kaplan-Meier database.

Single-cell analysis

CancerSEA (http://biocc.hrbmu.edu.cn/CancerSEA/home.jsp), a cancer single-cell database, was applied to reveal the correlation between GINS2 and 14 functional states in different tumor types.

University of Alabama Cancer Database (UALCAN) analysis

The online tool for gene expression and clinical data analysis UALCAN (http://ualcan.path.uab.edu/) was employed to explore the correlation between GINS2 expression and clinicopathological characteristics of HCC, including weight, nodal metastasis status, TP53 mutation status, tumor grade, histological subtype, cancer stage, gender, age, and race.

Multiple models on prognosis analysis

The ROC curve and time-dependent curve analyses were performed to investigate the performance of the prognostic classifier in predicting HCC patient outcome by estimating the AUC (area under the ROC curve) value. We also constructed univariate and multivariate cox regression models to explore the effect of various prognostic factors on overall survival (OS) of HCC patients.

Tissue specimens and cell lines

The HCC cell lines (HCC-LM3, SMMC-7721, MHCC-97L, and MHCC-97H) and immortalized non-cancerous hepatic LO2 cells were obtained from the Chinese Academy of Sciences (Shanghai, China). HUVECs were purchased from ATCC. HCC cells were maintained in DMEM (Gibco, USA) supplemented with 10% fetal bovine serum (FBS) (Gibco, USA). 45 paired (HCC and adjacent normal) tissues were obtained from patients undergoing hepatic resection at The First Affiliated Hospital of Nanjing Medical University. We obtained written informed consent from all the patients before the surgery. This research received ethics approval from the Ethics Committee of the First Affiliated Hospital of Nanjing Medical University. RNAlater solution (Thermo, USA) was used to save the tissue samples immediately after resection.

RT-qPCR analysis

Total RNA was isolated after cell lysis in TRIzol reagent (Invitrogen, USA). cDNA was obtained with the High Capacity cDNA Kit (Applied Biosystems, Germany). GAPDH served as an internal reference and the standard $2^{-\Delta\Delta CT}$ method was applied. The specific primers are shown in Table S1.

Cell treatment

Commercially available human LV-NC and LV-sh-GINS2 lentivirus were purchased from GenePharma (Shanghai, China). Transfected cells were selected by puromycin to generate stable cells. siRNAs targeting E2F1 were pur-

chased from Tsingke Biological Technology (Beijing, China). cDNAs encoding E2F1 and GINS2 were cloned into the pcDNA3.1 empty vector to consistently express E2F1 (pcDNA3.1-E2F1) or GINS2 (pcDNA3.1-GINS2). Lipofectamine 2000 reagent (Invitrogen, USA) was used in cell transfections according to the manufacturer's recommendations.

5-Ethynyl-2'-deoxyuridine (Edu) incorporation assay

The treated cells were plated into 24-well plates. The EdU assay kit (Ribobio) was conducted to assess cell proliferative ability. Briefly, after 2 h incubation with EdU, cells were stained with Apollo Dye Solution to label proliferating cells. Then, the cells were stained with DAPI. Images were captured with a fluorescence microscope.

CCK-8 assay and colony formation assay

1×10^3 treated cells were plated in each well of 96-well plates. Then, 10 μL of the CCK-8 (Doindo, Japan) solution was added to each well every 24 h. After 2 h incubation, optical density (OD) values at 450 nm were detected with a spectrophotometer. The treated cells were plated into each well of 6-well plates for colony-formation assay. Two weeks later, cells were fixed in 1% crystal violet for 1 h. Individual colonies were visualized and counted by the naked eye.

Flow cytometry analysis

Processed cells were fixed in pre-cooled ethanol under -20°C overnight. After washing three times to remove residual ethanol, cells were resuspended in 500 uL PI staining solution of the Cell Cycle Kit (MultiScience, China). After 30 min incubation, we used flow cytometry (FCM) to analyze the cell cycle.

Scratch-wound healing assay

The 8×10^5 stably transfected cells were plated into each well of the 6-well plates. A 200 μL sterile tip was used for wound scratching. Cells that have migrated were measured with phase-contrast microscopy at 0 h and 48 h.

Cell migration and invasion assays

For cell migration assays, the treated cells (2×10^4 cells/well) were seeded into the upper insert while the complete culture medium mixed with 20% FBS was added to the lower chambers. 24 h later, we washed the transwell membrane with PBS and stained the membrane with crystal violet solution. The migrated cells were imaged with a microscope. Similarly, cell invasion assays were performed using the Matrigel matrix-coated chamber, and cells were incubated for 48 h before staining.

Tube formation assay

Stably transfected 97H and LM3 cells were cultured with serum-free DMEM for 48 h and cell supernatants were collected and stored at -80°C. Then, 10 μL of Matrigel was pipetted into each well of 15-well plates (Ibidi, Germany) and polymerized for 30 min. Finally, a total of 50 μL conditional medium containing 1×10^4 HUVECs were planted into each well. After 4 h, the capillary-like structures were imaged using a microscope, and the number of capillary tubes was counted with ImageJ software.

Immunohistochemistry (IHC)

The collected subcutaneous and xenograft tumor tissues were fixed and then cut into sections. Each slide was incubated with antibodies specific for GINS2 or Ki-67 overnight at 4°C, followed by 1 h incubation with HRP-conjugated secondary antibodies. After that, a DAB kit was used to stain the slides. Subsequently, hematoxylin was used as a light nuclear counterstain. IHC staining signals were scored independently by both a pathologist and the author.

Western blot

The cell lysis buffer was used to extract the total proteins from HCC tissues and cells. The samples were then mixed with loading buffer, resolved by SDS-PAGE gel, and transferred onto PVDF membranes (Millipore, USA). Subsequently, the membranes were probed with appropriate primary antibodies and visualized by the ECL detection system (Millipore, USA). The primary antibodies used in this study is provided in Table S2.

Chromatin immunoprecipitation assay (ChIP)

The ChIP assay was conducted with the Magna ChIP assay kit (Millipore, USA). 97H and LM3 cells were fixed with 1% formaldehyde to cross-link proteins and DNA. Cell lysates were then subjected to immunoprecipitation with either

the negative control IgG or anti-E2F1 antibodies at 4°C overnight with constant rotation. Finally, the amount of co-precipitated DNA was detected by qRT-PCR. Primer sequences for the ChIP assay are shown in Table S3.

In vivo tumorigenesis and metastasis assays

For the subcutaneous xenograft study, ten mice (5-week-old, female, BALB/c) were randomly grouped into two groups. Then, HCC cell lines LM3 that inhibited expression of GINS2 were inoculated into the left flank of nude mice (2×10^6 cells/200 μl). We recorded and assessed the xenograft using the formula: volume = $0.5 \times (\text{length} \times \text{width}^2)$. Four weeks after injection, the xenografts were harvested, weighed, and fixed.

For *in vivo* tumor metastasis assays, twelve mice were randomly grouped into two groups. A total of 2×10^6 cells were injected into the tail veins of nude mice. After eight weeks, each mouse was injected with 100 mg/kg D-luciferin (Yisheng, China) and evaluated using the Berthold Imaging System (Berthold, Germany). Then, the mice were sacrificed and their lungs analyzed by HE staining. All experiments and animal handling were conducted following the guidelines of Nanjing Medical University Institutional Animal Care Committee.

Dual-luciferase reporter assay

Cells were transfected with appropriate plasmids using Lipofectamine 2000 (Thermo Fisher Scientific, USA). After 48 h, luciferase activities were detected with the Dual Luciferase Reporter Assay system (Beyotime).

Statistical analyses

Data were analyzed using GraphPad Prism5 (GraphPad Software) and presented as mean ± S.D. Each experiment was conducted with at least three independent biological replicates. A p-value < 0.05 was considered statistically significant.

Results

GINS2 was upregulated in HCC tissues

To investigate whether GINS2 was dysregulated in HCC tissues, we first examined its expression using the TIMER online database. GINS2 was upregulated in 17 cancer types including HCC (**Figure 1A**). Then, TCGA and HCCDB databases were examined to further explore the GINS2 expression in HCC. As shown in **Figure 1B** and **1C**, GINS2 was significantly elevated in HCC tumor tissues. The results of RT-qPCR, western blot, and IHC analysis further confirmed the high expression of GINS2 in HCC tissues. (**Figure 6A**, **6D**, and **6E**). Moreover, we also demonstrated GINS2 expression was higher in HCC cells (SMMC-7721, MHCC-97L, MHCC-LM3, and Huh7) compared to LO2 liver cells, particularly in 97H and LM3 cells (**Figure 6B**). Subsequent survival analysis by the Kaplan-Meier plotter database illustrated that higher GINS2 expression correlated with poor OS, PFS, DSS, and RFS of HCC patients (**Figure 1D**).

GINS2 expression and clinicopathologic features of HCC patients

To explore the correlation between GINS2 and clinicopathologic features in HCC tissues, we downloaded the clinical data of LIHC in TCGA database. As illustrated in **Table 1**, GINS2 expression was associated with the Pathologic stage, T stage, Histologic grade, and AFP level of HCC patients. The outcome of logistic regression analysis also indicated that upregulated GINS2 expression was significantly associated with T stage, Pathologic stage, Tumor status, and Histologic grade in HCC (Table S4). Furthermore, the UALCAN database was employed to explore GINS2 expression in subgroups of patients based on different clinical features. For tumor grade, High GINS2 expression was observed in HCC patients in grade 1, 2, 3, and 4 (**Figure 2A**). In terms of individual cancer stages, GINS2 expression was significantly upregulated in stages 1, 2, and 3 (**Figure 2B**). Analysis of the node metastasis status showed that GINS2 expression was significantly elevated in the N0 group of HCC patients. Notably, GINS2 expression in N0 and N1 groups was not statistically significant due to the smaller sample in the N1 group (**Figure 2C**). TNMplot was then employed to further assess the association between GINS2 expression and metastasis status of HCC patients [19], and the results are presented in Figure S1. Interestingly, we found GINS2 expression was significantly increased in TP53-mutant and wild-type HCC patients (**Figure 2D**). Further analysis indicated that upregulated GINS2 expression was inde-

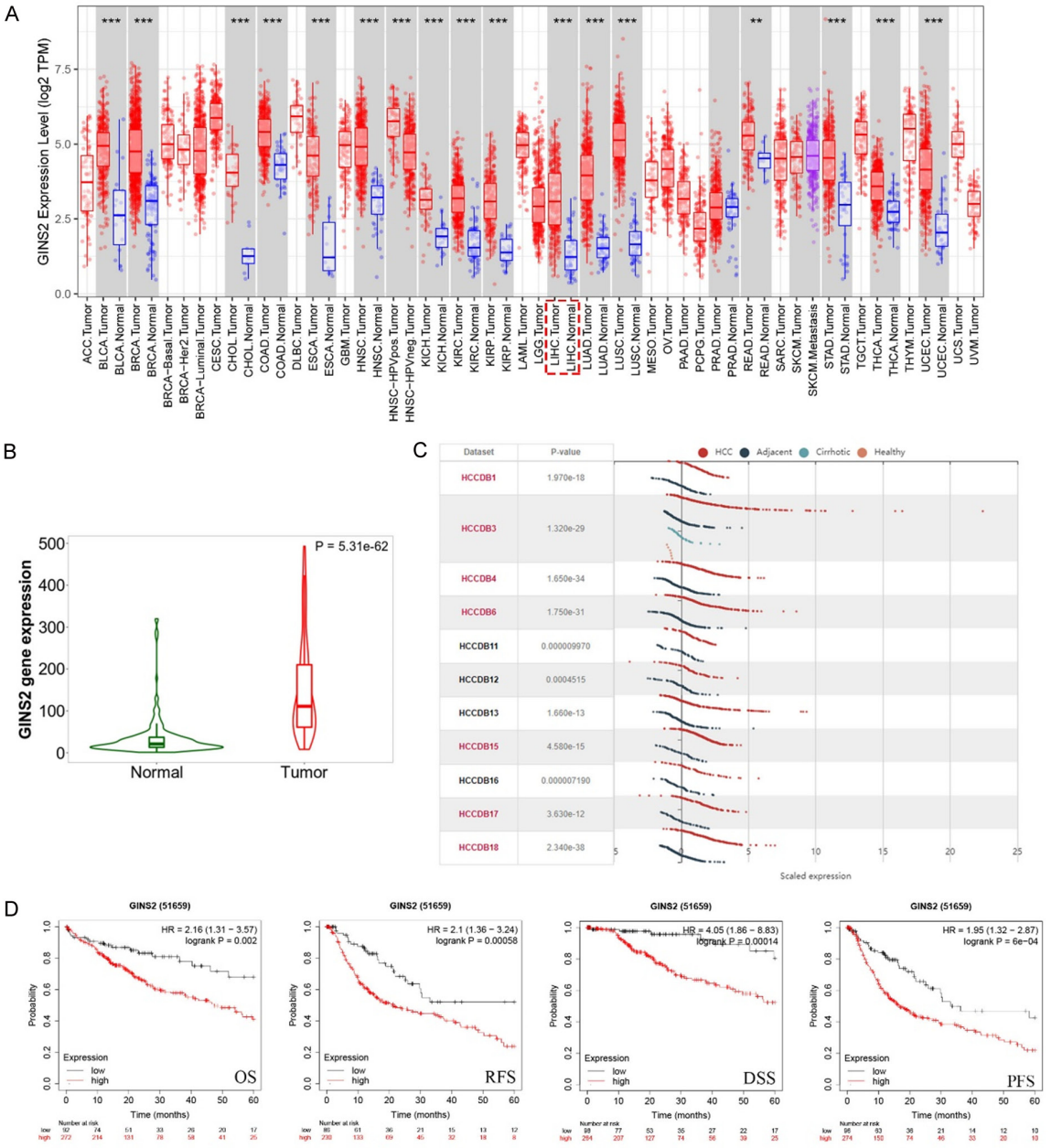

Figure 1. GINS2 expression levels in HCC from TIMER and HCCDB databases. A. Expression levels of GINS2 in pan-cancers from the TIMER database. B. Violin plot of GINS2 expression between HCC tissues and adjacent healthy tissues according to the TCGA database. C. Expression levels of GINS2 in HCC tissues and adjacent healthy tissues according to the HCCDB database. D. Kaplan-Meier survival curve analysis of the prognostic significance of GINS2 expression based on the Kaplan-Meier database. *P < 0.05; **P < 0.01; ***P < 0.001. (ACC, BLCA, CESC, CHOL, COAD, DLBC, ESCA, GBM, HNSC, KICH, KIRC, KIRP, LAML, LGG, LIHC, LUAD, LUSC, MESO, OV, PAAD, PCPG, PRAD, READ, SARC, SKCM, SKCM, TGCT, HCA, THYM, UCEC, UCS, UVM).

pendent of patients' gender, age, race, weight, or histological subtypes (Figure S1).

The prognostic value of GINS2 in HCC

We found the area under curves (AUC) of receiver operator characteristic (ROC) curve was 0.909, suggesting the ability of using GINS2 expression to accurately distinguish tumors from normal ones (**Figure 3A**). The time-dependent ROC curve analysis of GINS2 was also performed to predict overall survival of HCC. As illustrated in **Figure 3B**, AUC values of one-, three-, and five-year overall survival were above

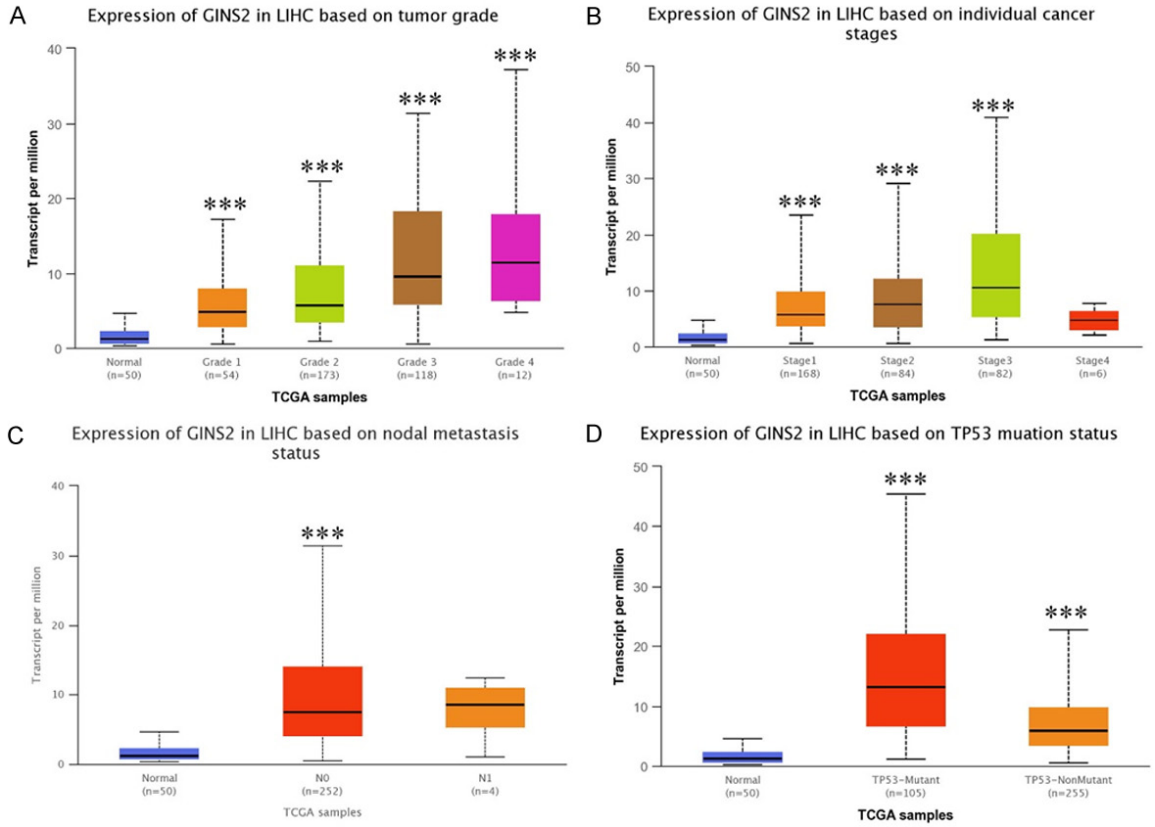

Figure 2. Box plot evaluation of GINS2 expression in subgroups of LIHC samples (UALCAN). Upregulated mRNA of GINS2 is independent of patients' tumor grade (A), cancer stage (B), nodal metastasis status (C), and TP53 mutation status (D). The t-test was used to estimate the significance of differences in gene expression levels between groups. *P < 0.05; **P < 0.01; ***P < 0.001.

0.6, which is considered suitable for prediction. In addition, the results of univariate regression analysis illustrated that T stage, Pathologic stage, Tumor status, and GINS2 expression all significantly correlated with HCC patient OS (**Figure 3C** and Table S5). Finally, GINS2 expression and Tumor status were selected as independent prognostic factors for patients with HCC according to the multivariate regression analysis (**Figure 3D** and Table S5). These results helped shed light on the prognostic value of GINS2.

The correlation between GINS2 expression and immune cell infiltration

Recently, numerous studies have indicated the importance of immune cell infiltration in HCC occurrence and development [20-22]. Therefore, we assessed the potential correlation between GINS2 expression and immune cell markers in HCC using the TIMER2.0 database. As shown in **Figure 4A**, GINS2 expression was positively correlated with the infiltration of B cells, CD8+ T cells, macrophages, and dendritic cells in HCC tissues. Then, we carried out ssGSEA to further explore the immune cell infiltration landscape of HCC (recorded as ssGSEA score) according to the expression of GINS2. The results indicated a close relationship between GINS2 expression and immune cell infiltration (**Figure 4B**). Besides, the heat map was plotted to show the correlation between different tumor-infiltrating immune cells (**Figure 4C**).

PPI, GO, and KEGG analysis of GINS2

A comprehensive protein-protein interaction network of GINS2 was constructed with the GeneMANIA database (**Figure 5A**), which revealed interactions between GINS1, GINS2, GINS3, GINS4, and MCM2-7. This is consistent with previously published studies [8, 9]. Then, we conducted single-cell analysis to examine the association between GINS2 and 14 func-

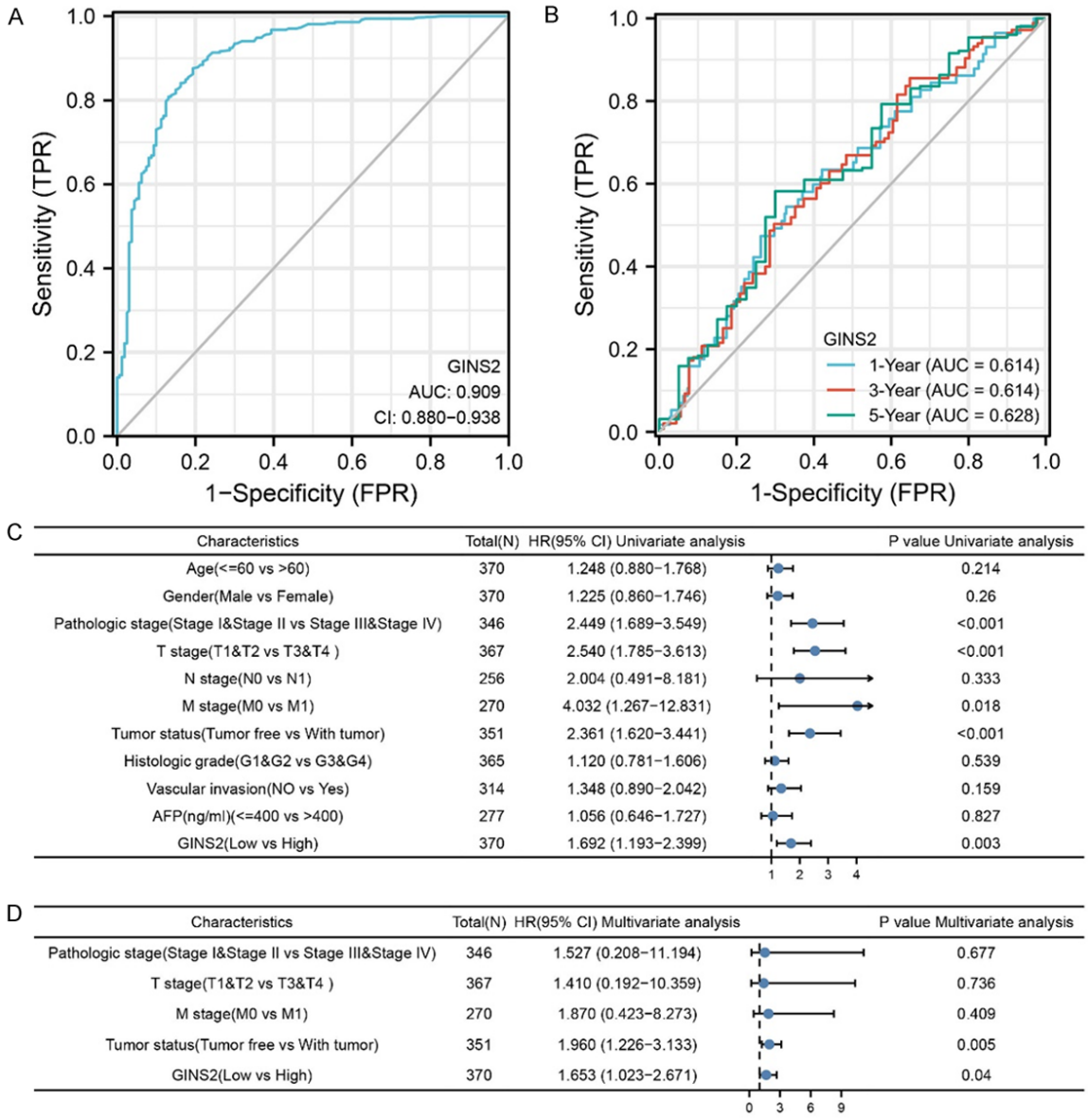

Figure 3. GINS2 expression and other clinicopathologic factors with OS in LIHC were calculated via univariate and multivariate regression analysis. A. The ROC curve of diagnosis to distinguish tumor from normal tissue. The AUC was 0.909. B. Time-dependent survival ROC curve analysis to predict 1-, 3-, and 5-year survival rates. C. The forest plot of univariate regression analysis. Among the factors, T stage, Pathologic stage, Tumor status, and GINS2 expression were identified as statistically significantly associated with the likelihood for OS univariate analysis. D. The forest plot of multivariate regression analysis.

tional states in various cancer types. As illustrated in **Figure 5B**, GINS2 expression was positively associated with invasion, cell cycle, DNA repair, DNA damage, and proliferation. GO and KEGG analysis was next performed with genes co-expressed with GINS2 according to the LinkedOmics online tool. The enriched KEGG pathways illustrated that these co-expressed genes were mainly associated with cell cycle and DNA replication (**Figure 5C**). Meanwhile, GO function annotation was mainly enriched in nuclear division, DNA replication, and regulation of cell cycle phase transition (**Figure 5D**).

Knockdown of GINS2 induced cell proliferation restriction and cell cycle arrest of HCC cells

Stably transfected 97H and LM3 cell lines were generated using Lenti-sh-GINS2 or Lenti-sh-NC constructs. RT-qPCR and western blot experiments were performed to confirm the knock-

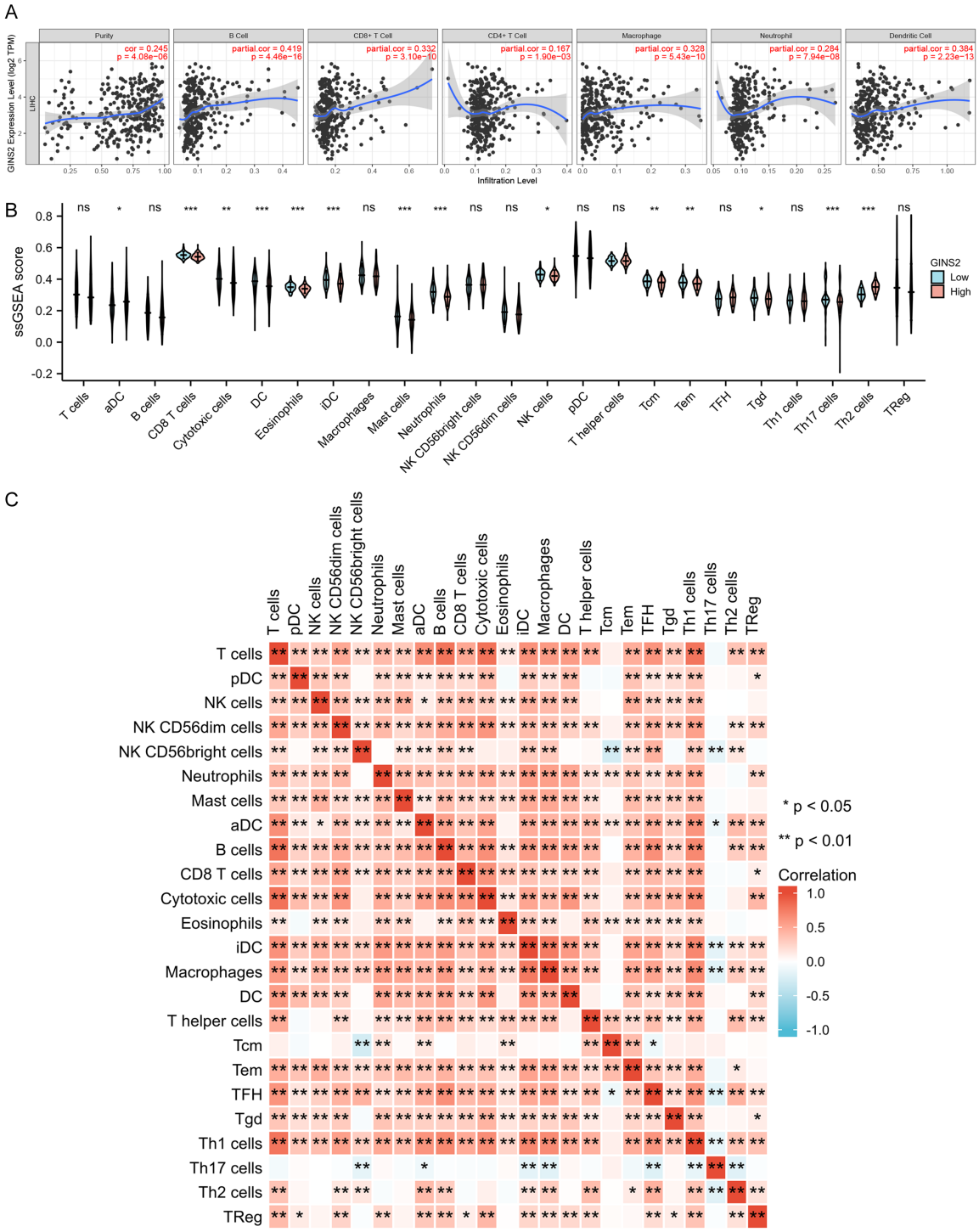

Figure 4. Correlations between GINS2 expression and immune infiltration level in HCC. A. The expression of GINS2 was significantly correlated with infiltrating levels of B cell, CD8+ T cells, CD4+ T cells, macrophages, neutrophils, and dendritic cells in HCC. B. The varied proportions of 24 subtypes of immune cells in high and low GINS2 expression groups in tumor samples. C. Heatmap of 24 immune infiltration cells in tumor samples. *P < 0.05; **P < 0.01; ***P < 0.001.

down efficiency. As illustrated in **Figure 6G** and **6H**, the expression of GINS2 decreased the most in the sh1 group. CCK-8, Edu, and colony formation assays were subsequently conducted to assess the effect of GINS2 on cell proliferation. Data from these experiments revealed

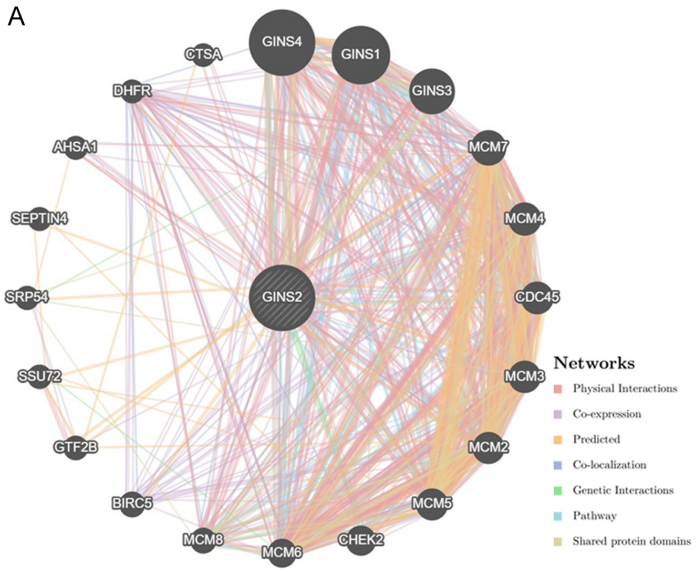
A
GINS4
GINS1
GINS3
CTSA
DHFR
AHSA1
MCM7
SEPTIN4
MCM4
SRP54
GINS2
CDC45
SSU72
MCM3
GTF2B
MCM2
BIRC5
MCM5
MCM8
MCM6
CHEK2
Networks
Physical Interactions
Co-expression
Predicted
Co-localization
Genetic Interactions
Pathway
Shared protein domains

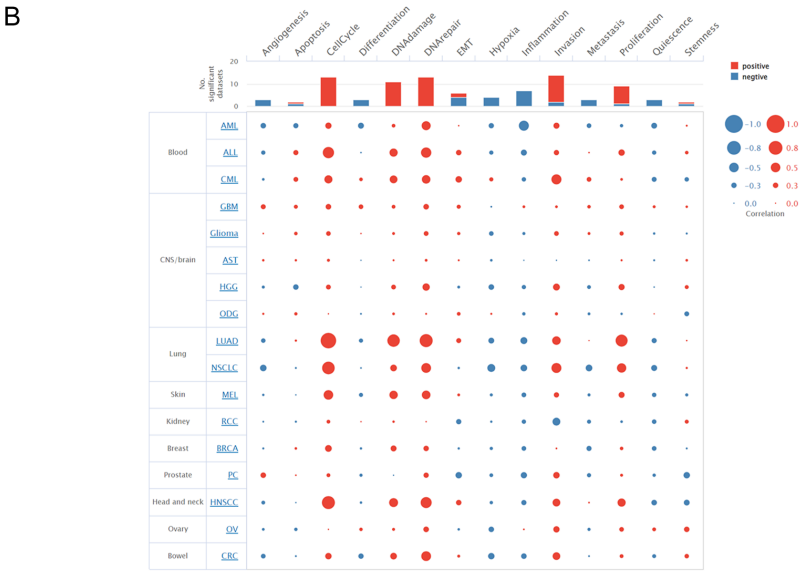
B
Angiogenesis
Apoptosis
CellCycle
Differentiation
DNAdamage
DNArepair
EMT
Hypoxia
Inflammation
Invasion
Metastasis
Proliferation
Quiescence
Stemness
No. significant datasets
positive
negtive
Correlation
Blood
AML
ALL
CML
CNS/brain
GBM
Glioma
AST
HGG
ODG
Lung
LUAD
NSCLC
Skin
MEL
Kidney
RCC
Breast
BRCA
Prostate
PC
Head and neck
HNSCC
Ovary
OV
Bowel
CRC

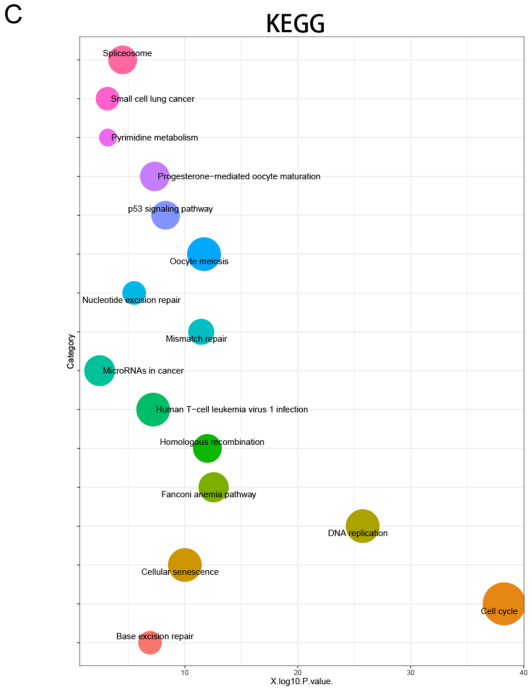
C
KEGG
Spliceosome
Small cell lung cancer
Pyrimidine metabolism
Progesterone−mediated oocyte maturation
p53 signaling pathway
Oocyte meiosis
Nucleotide excision repair
Mismatch repair
MicroRNAs in cancer
Human T−cell leukemia virus 1 infection
Homologous recombination
Fanconi anemia pathway
DNA replication
Cellular senescence
Cell cycle
Base excision repair
Category
X.log10.P.value.

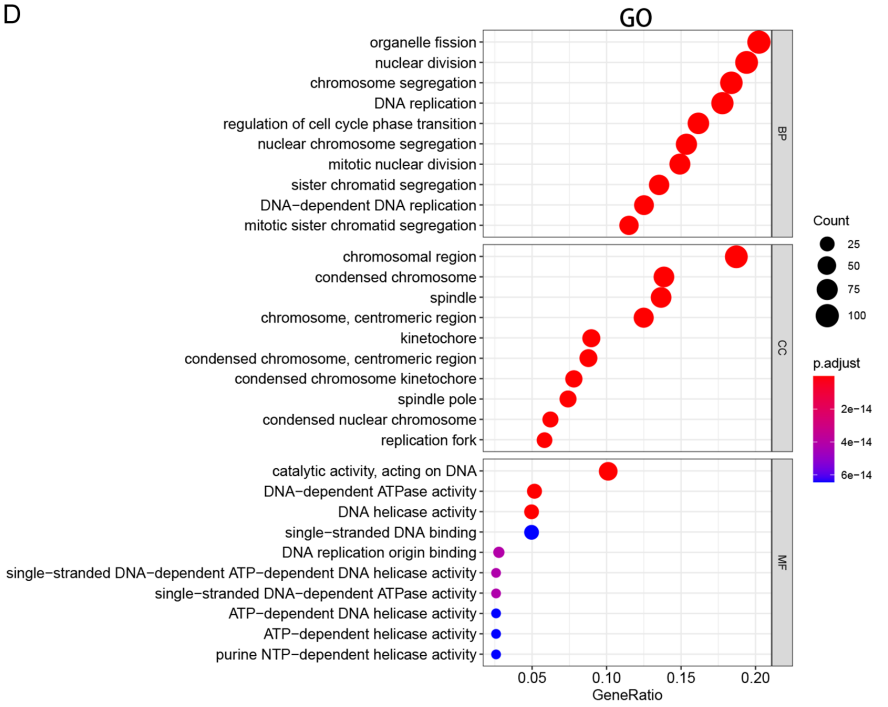
D
GO
organelle fission
nuclear division
chromosome segregation
DNA replication
regulation of cell cycle phase transition
nuclear chromosome segregation
mitotic nuclear division
sister chromatid segregation
DNA−dependent DNA replication
mitotic sister chromatid segregation
BP
chromosomal region
condensed chromosome
spindle
chromosome, centromeric region
kinetochore
condensed chromosome, centromeric region
condensed chromosome kinetochore
spindle pole
condensed nuclear chromosome
replication fork
CC
catalytic activity, acting on DNA
DNA−dependent ATPase activity
DNA helicase activity
single−stranded DNA binding
DNA replication origin binding
single−stranded DNA−dependent ATP−dependent DNA helicase activity
single−stranded DNA−dependent ATPase activity
ATP−dependent DNA helicase activity
ATP−dependent helicase activity
purine NTP−dependent helicase activity
MF
GeneRatio
Count
p.adjust

Figure 5. PPI, GO and KEGG analysis of the genes co-expressed with GINS2 in HCC. A. The protein-protein interaction network of GINS2 was constructed using GeneMANIA. B. Single-cell analysis displayed the correlation between GINS2 and 14 functional states (including angiogenesis, apoptosis, cell cycle, differentiation, DNA damage, DNA repair, EMT, hypoxia, inflammation, invasion, metastasis, proliferation, stemness, and quiescence) in different tumor types. C, D. Significantly enriched KEGG pathways and GO annotations of the genes co-expressed with GINS2 in HCC based on the LinkedOmics database.

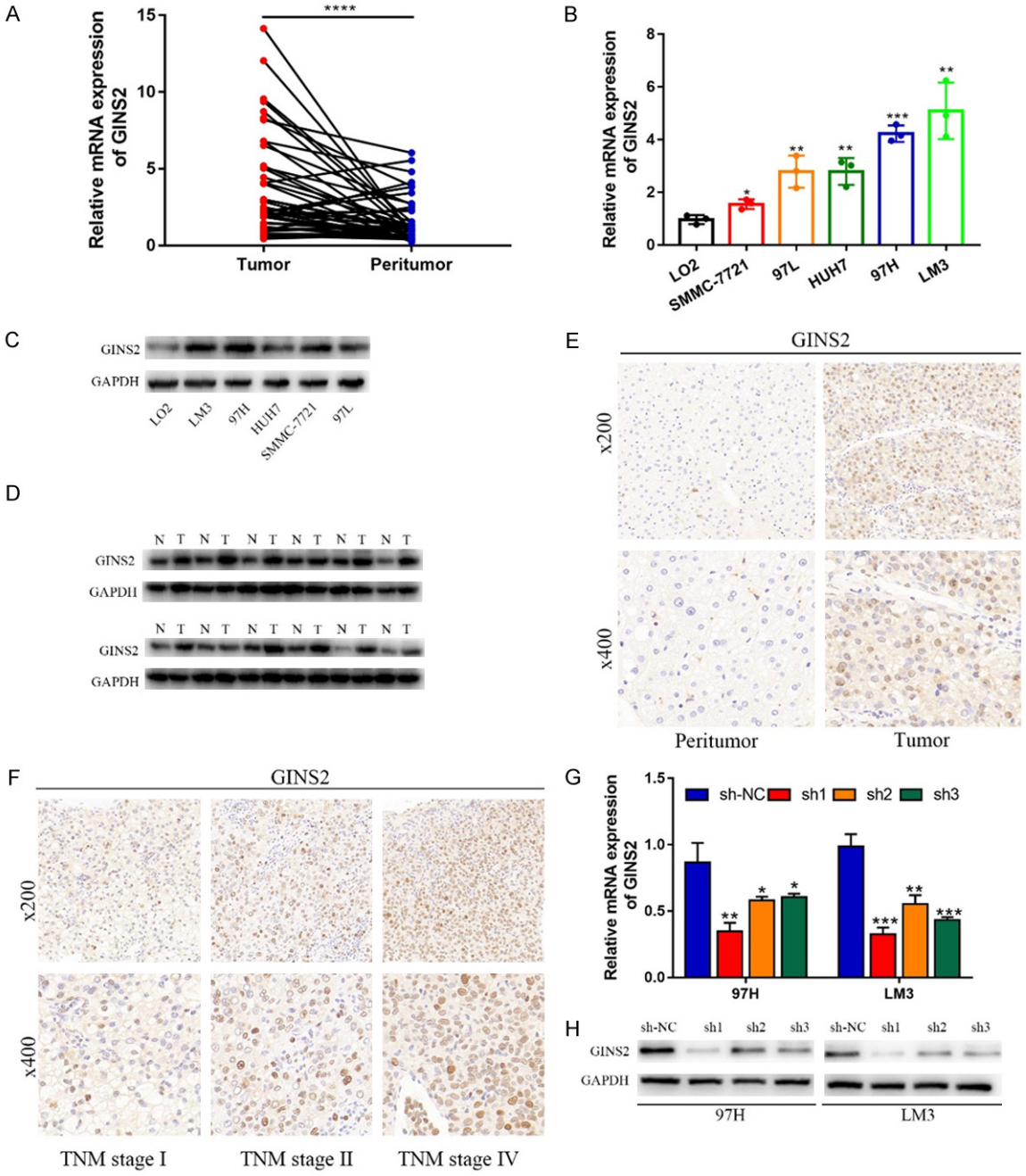

Figure 6. GINS2 expression decreased in HCC tissue samples and cell lines. A. qRT-PCR was used to examine the expression of GINS2 in 45 pairs of HCC tissues and corresponding peritumor tissues. B. The mRNA expression levels of GINS2 in HCC cell lines and normal LO2 cells. C, D. Western blot showing that GINS2 was upregulated in HCC tissues and HCC cell lines compared with adjacent healthy tissues and LO2 cells. E, F. The protein level of GINS2 in HCC specimens and adjacent normal tissues was detected by IHC. G, H. GINS2 knockdown efficiency was analyzed by qRT-PCR and western blot. All data are represented as mean ± S.E.M. *P < 0.05; **P < 0.01; ***P < 0.001.

Table 1. Association between GINS2 expression and clinicopathologic features in HCC samples from the TCGA database

Characteristic	Low expression of GINS2	High expression of GINS2	*P*-value
n	185	186	
Age, n (%)			0.405
≤ 60	84 (22.7%)	93 (25.1%)	
> 60	101 (27.3%)	92 (24.9%)	
Gender, n (%)			0.530
Female	57 (15.4%)	64 (17.3%)	
Male	128 (34.5%)	122 (32.9%)	
Pathologic stage, n (%)			0.012
Stage I	97 (28%)	74 (21.3%)	
Stage II	40 (11.5%)	46 (13.3%)	
Stage III	32 (9.2%)	53 (15.3%)	
Stage IV	4 (1.2%)	1 (0.3%)	
T stage, n (%)			0.027
T1	104 (28.3%)	77 (20.9%)	
T2	42 (11.4%)	52 (14.1%)	
T3	31 (8.4%)	49 (13.3%)	
T4	6 (1.6%)	7 (1.9%)	
N stage, n (%)			1.000
N0	122 (47.7%)	130 (50.8%)	
N1	2 (0.8%)	2 (0.8%)	
M stage, n (%)			0.361
M0	129 (47.8%)	137 (50.7%)	
M1	3 (1.1%)	1 (0.4%)	
Histologic grade, n (%)			< 0.001
G1	34 (9.3%)	21 (5.7%)	
G2	100 (27.3%)	77 (21%)	
G3	44 (12%)	78 (21.3%)	
G4	4 (1.1%)	8 (2.2%)	
AFP (ng/ml), n (%)			0.014
≤ 400	118 (42.4%)	95 (34.2%)	
> 400	24 (8.6%)	41 (14.7%)	
Child-Pugh grade, n (%)			0.573
A	110 (46%)	107 (44.8%)	
B	12 (5%)	9 (3.8%)	
C	0 (0%)	1 (0.4%)	
Vascular invasion, n (%)			0.249
No	110 (34.9%)	96 (30.5%)	
Yes	50 (15.9%)	59 (18.7%)	

that downregulating GINS2 suppressed the proliferative ability of 97H and LM3 cells (**Figure 7A-C**; Figure S2A). Moreover, cell cycle analysis demonstrated that depleting GINS2 resulted in a substantial increase in the G0/G1 phase (**Figure 7D**). Collectively, these findings demonstrated that silencing GINS2 could significantly suppress cell viability and induce G1 phase cell cycle arrest in HCC cells.

Knockdown of GINS2 inhibited migration and invasion of HCC cells

Given the positive correlation between GINS2 expression and the metastasis status in HCC patients, we hypothesized that GINS2 might facilitate the migration and invasion of HCC cells. Both wound healing assays and transwell assays showed the suppressed invasion and migration of 97H and LM3 cells, following GINS2 knockdown. (**Figure 8A**, **8B** and Figure S2B). Additionally, we found that co-culturing with GINS2-silenced cells significantly suppressed the migration, invasion, and tube formation of HUVECs (**Figure 8C**). Furthermore, a significant decrease was observed in the proteins associated with angiogenesis (VEGF) and cell cycle (CCND1, CDK2, and CDK4) in GINS2-silenced cells (**Figure 8D**). Taken together, our results illustrated that GINS2 could increase cell migration and invasion capabilities and affect the angiogenesis, invasion, and migration of HUVECs, which may ultimately lead to enhanced metastasis of HCC.

GINS2 accelerated the proliferation and metastasis of HCC cells in mouse models

Xenograft tumors were generated in nude mice to evaluate GINS2 in vivo. Compared with the control group, tumors from GINS2-silenced cells showed a marked decrease in tumor growth (**Figure 9A-C**). Immunohistochemistry staining with an anti-Ki67 antibody in xenograft tumors showed similar results (**Figure 9D**). A metastatic xenograft model was next generated by lateral tail-vein injection of

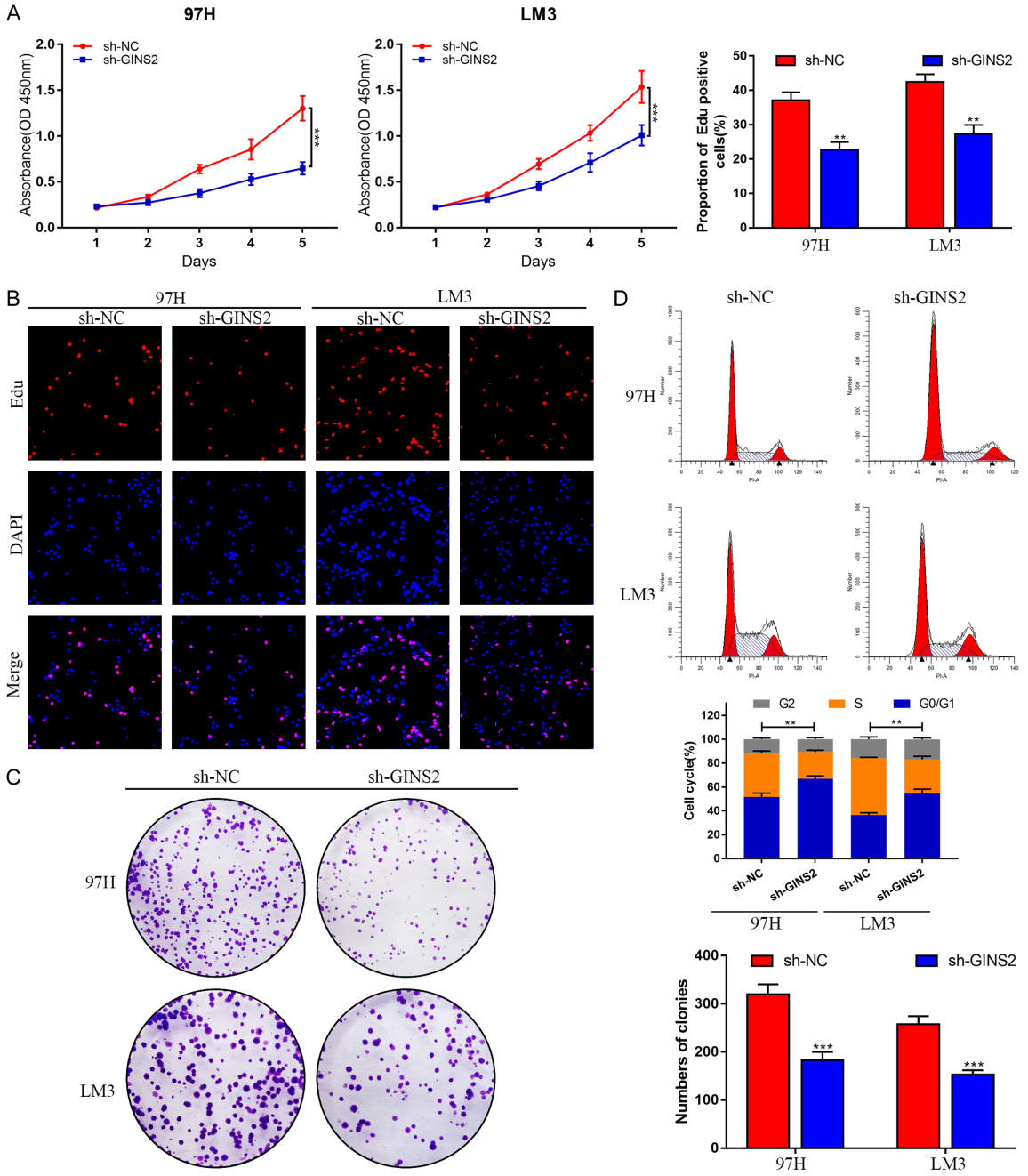

Figure 7. Knockdown of GINS2 suppresses cell proliferation and induces cell cycle arrest of HCC cells *in vitro*. A. CCK-8 assay was performed in 97H and LM3 cells transfected with sh-NC or sh-GINS2. B. Cell proliferation was further examined in sh-NC and sh-GINS2 cells by EdU assay. C. The effect of GINS2 on colony-forming ability was detected by colony formation assay in 97H and LM3 cells after transfection. D. Flow cytometry results show the cell cycle distribution of GINS2 silenced 97H and LM3 cells. All data are represented as mean ± S.E.M. *P < 0.05; **P < 0.01; ***P < 0.001.

LM3 cells. Mice were anesthetized after eight weeks to obtain lung tissues. The tissues were then subjected to HE staining, which showed decreased metastatic nodules in the GINS2-silencing group compared to the control group (**Figure 9E**).

GINS2 was transcriptionally activated by E2F1 in HCC cells

Previous studies have defined transcription factors (TFs) as key regulators of gene expression [23, 24]. The hTFtarget database was used to

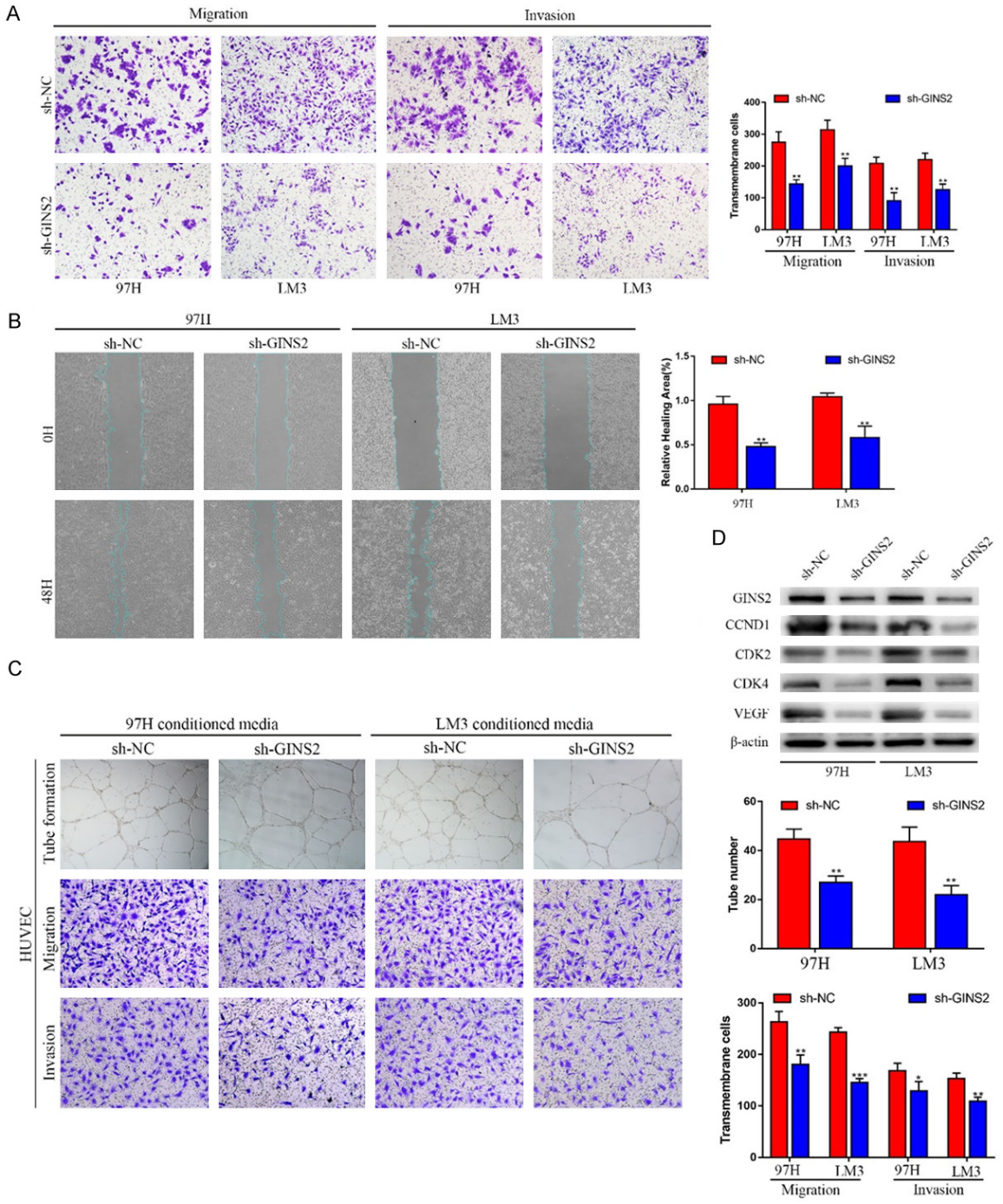

Figure 8. Knockdown of GINS2 suppresses invasion and migration of HCC cells *in vitro*. A. Invasive or migrated cells were measured by transwell assays with or without Matrigel. B. Wound-healing migration assays detected the effects of silencing GINS2 on cell migration. C. Tube formation, invasion, and migration of HUVECs in sh-GINS2 cell culture medium. D. Western blot analysis of cell angiogenesis and cell cycle-related proteins in 97H or LM3 cells with or without GINS2 knockdown. All data are represented as mean ± S.E.M. *P < 0.05; **P < 0.01; ***P < 0.001.

predict potential TFs that could regulate GINS2 expression. E2F1 and E2F7 were selected for further study by plotting Venn diagrams of three gene lists: TFs predicted by the hTFtarget database, upregulated genes in LIHC according to TCGA data, and genes positively correlated with GINS2 expression in HCC according to the LinkedOmics database (**Figure 10A**). The analy-

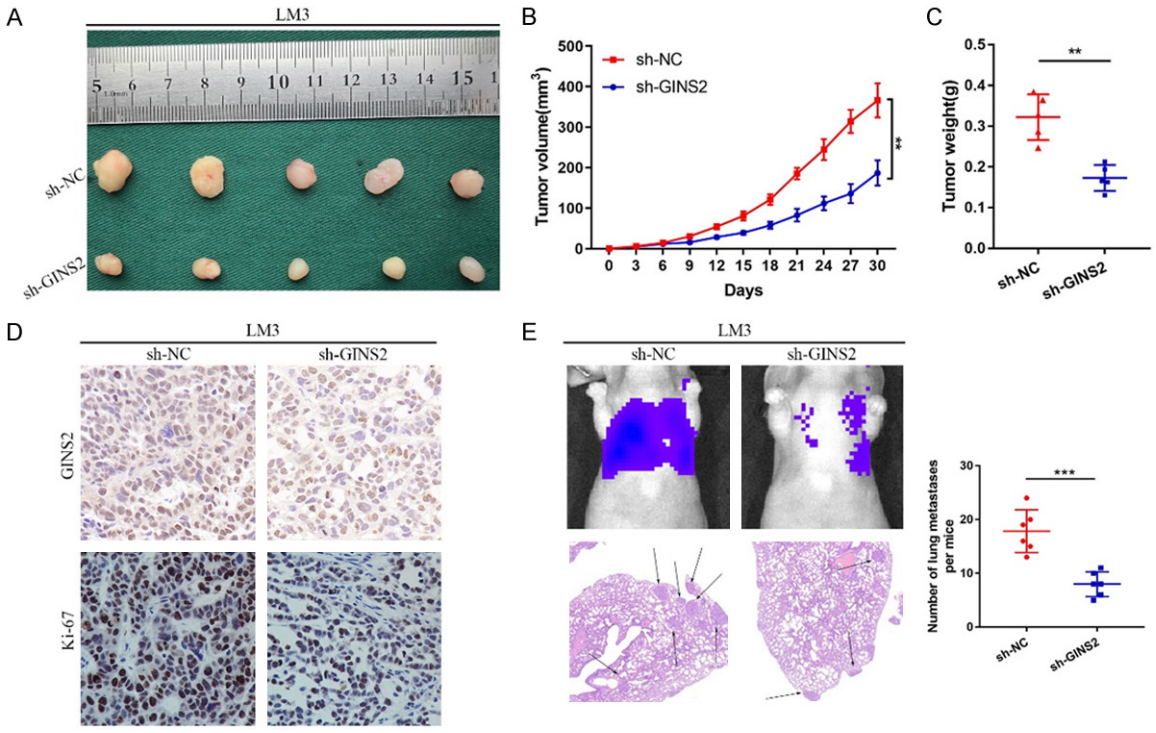

Figure 9. GINS2 promotes HCC progression *in vivo*. LM3 cells infected by sh-GINS2 or negative control sh-NC lentiviruses were implanted into nude mice and tumor growth was recorded. A-C. Images of tumors from different groups of nude mice. Tumor volume and average weight were assessed. D. IHC analysis of GINS2 and Ki-67 in the tumors derived from mice. E. GINS2 stable knockdown LM3 cells were injected into the tail vein of nude mice to induce lung metastasis. The relative luciferase activity of HCC tumor in nude mice from the sh-NC or sh-GINS2 group were determined using a live imaging system. Liver metastatic nodules were subjected to HE staining as indicated. All data are presented as mean ± S.E.M. *P < 0.05; **P < 0.01; ***P < 0.001.

sis indicated a strong correlation between E2F1 and GINS2 in the TCGA, GTEx, and CCLE databases (**Figure 10B-D** and Figure S3). Moreover, E2F1 expression in HCC tissues was higher than in non-tumor tissues, where higher levels of E2F1 indicated poorer outcome in HCC patients (**Figure 10E** and **10F**). Therefore, we chose E2F1 for further research.

Using the JASPAR database, we acquired the first three E2F1-binding sequences from the promoter regions of GINS2 (**Figure 10G** and Figure S4). In addition, we demonstrated a potential regulatory relationship between E2F1 and GINS2 by knocking down or overexpressing E2F1 in 97H and LM3 cells, the efficiencies of which were further verified by qRT-PCR and western blot (**Figure 10H** and **10I**). Chromatin immunoprecipitation (ChIP) assays also confirmed the predicted binding sites. Collectively, the data showed that E2 was the binding site of E2F1 on the GINS2 promoter region (**Figure 10J**). Subsequently, E2F1 overexpression could significantly drive the luciferase activity of GINS2 promoter-E2-Wt (**Figure 10K**). The above findings indicate that E2F1 could activate the transcription of GINS2 via binding to the GINS2 promoter region in HCC cells.

GINS2 could promote proliferative, migratory, and invasive capabilities of HCC cells through regulating the PI3K/AKT/mTOR signaling pathway

To find out the cellular mechanism of GINS2's role in HCC progression, we analyzed the correlation between GINS2 and 50 signaling pathways in hallmark gene sets downloaded from the MsigDB database, which demonstrated that GINS2 expression was positively associated with HALLMARK_PI3K_AKT_MTOR_SIGNALING in most cancers types including HCC (**Figure 11A** and **11B**). Therefore, we surmised that GINS2 could activate the PI3K/AKT/mTOR pathway. Western blot analysis indicated that knockdown of GINS2 inhibited levels of phos-

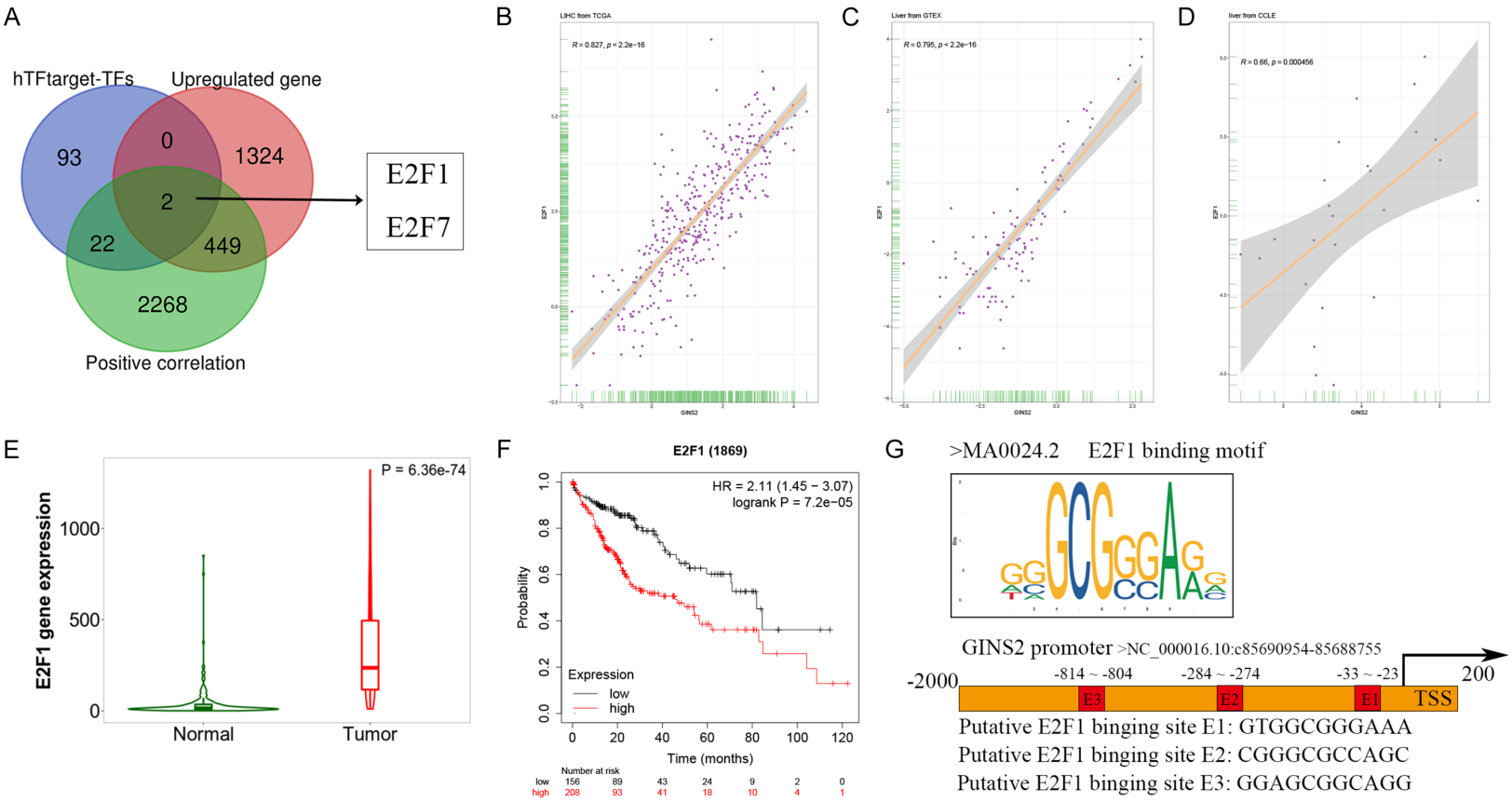
A
hTFtarget-TFs
Upregulated gene
93
0
1324
2
22
449
2268
Positive correlation
E2F1
E2F7
B
LIHC from TCGA
R = 0.827, p < 2.2e−16
C
Liver from GTEX
R = 0.795, p < 2.2e−16
D
liver from CCLE
R = 0.66, p = 0.000456
E
E2F1 gene expression
P = 6.36e-74
Normal
Tumor
F
E2F1 (1869)
HR = 2.11 (1.45 − 3.07)
logrank P = 7.2e−05
Probability
Expression
low
high
Time (months)
Number at risk
low 156 89 43 24 9 2 0
high 208 93 41 18 10 4 1
G
>MA0024.2 E2F1 binding motif
GINS2 promoter >NC_000016.10:c85690954-85688755
-2000
-814 ~ -804
-284 ~ -274
-33 ~ -23
200
E3
E2
E1
TSS
Putative E2F1 binging site E1: GTGGCGGGAAA
Putative E2F1 binging site E2: CGGGCGCCAGC
Putative E2F1 binging site E3: GGAGCGGCAGG

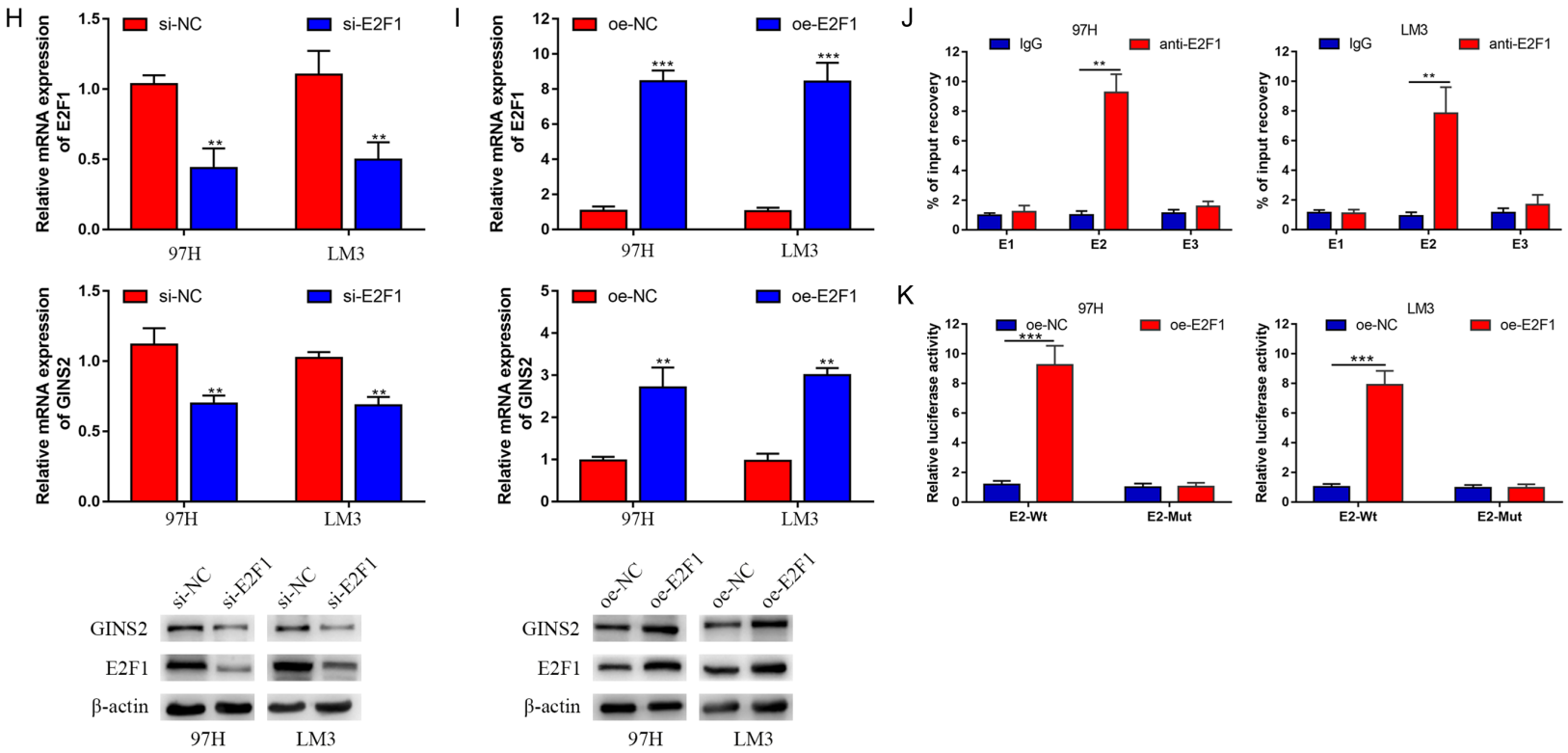

Figure 10. GINS2 was transcriptionally activated by E2F1. A. Venn diagrams of three gene lists: transcription factors predicted by the hTFtarget database, upregulated genes in LIHC according to the data from TCGA database, genes positively correlated with GINS2 expression in HCC according to the LinkedOmics database. B-D. Correlation between E2F1 and GINS2 in the TCGA, GTEx, and CCLE databases. E. Violin plot of E2F1 expression between HCC tissues and adjacent healthy tissues according to data from the TCGA database. F. Kaplan-Meier survival curve analysis of the prognostic significance of E2F1 expression based on the Kaplan-Meier database. G. E2F1-binding motifs and predicted E2F1-binding sites (E1, E2, and E3) on the promoter region of GINS2 were obtained from the JASPAR database. H, I. Expression of E2F1 and GINS2 was confirmed by qRT-PCR or western blot in 97H and LM3 cells transfected with si-E2F1, si-NC, pcDNA3.1, or pcDNA3.1-E2F1. J. qRT-PCR analysis of ChIP products validated the binding capacity of E2F1 to the GINS2 promoter. K. The luciferase reporter assay further confirmed direct binding of E2F1 to the GINS2 promoter in 97H and LM3 cells transfected with pcDNA3.1 or pcDNA3.1-E2F1. All data are presented as mean ± S.E.M. *P < 0.05; **P < 0.01; ***P < 0.001.

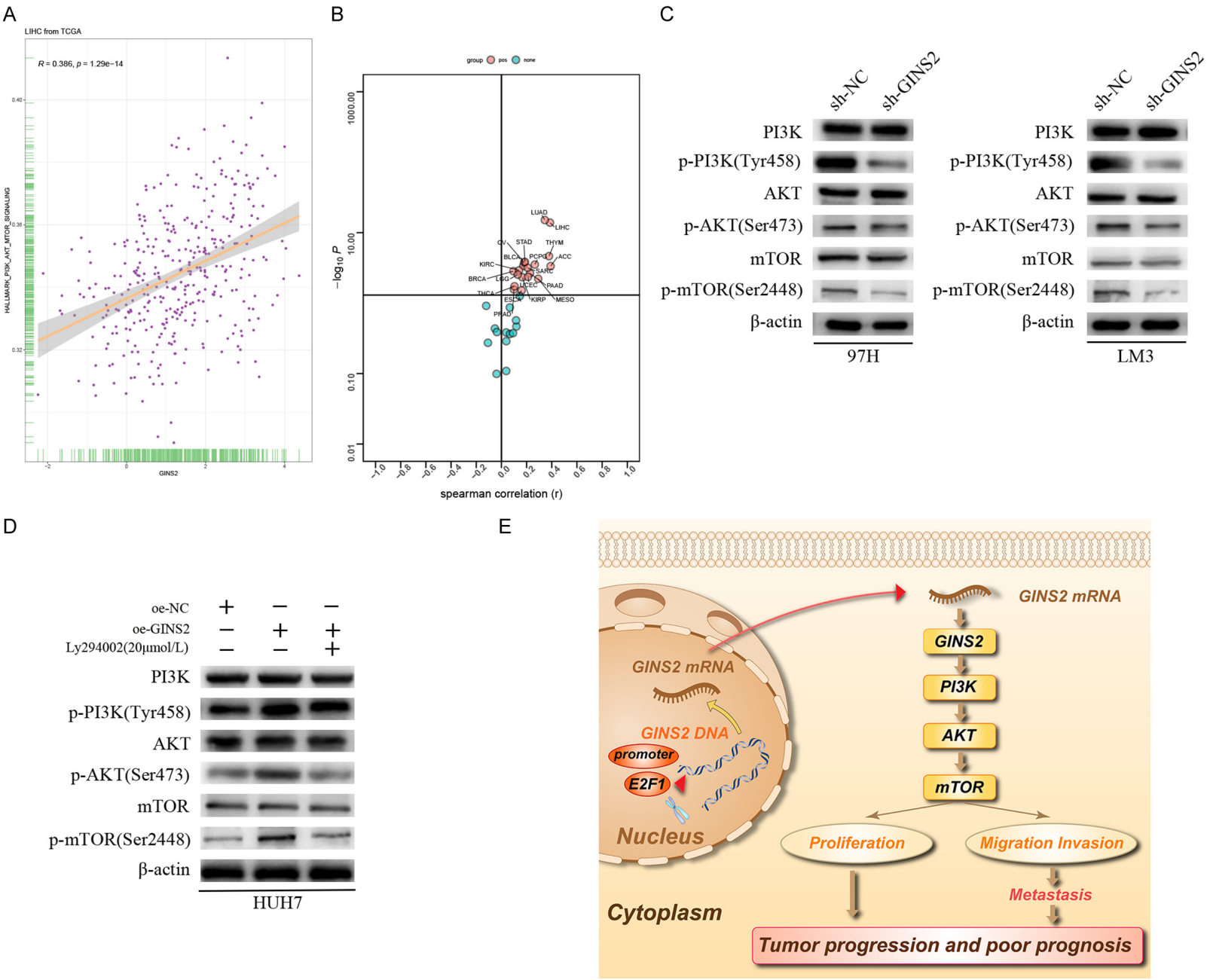
A
LIHC from TCGA
R = 0.386, p = 1.29e−14
HALLMARK_PI3K_AKT_MTOR_SIGNALING
GINS2
B
group pos none
−log10 P
spearman correlation (r)
LUAD
LIHC
CV
STAD
THYM
BLCA
PCPG
ACC
KIRC
SARC
BRCA
LGG
UCEC
PAAD
THCA
ESCA
KIRP
MESO
PRAD
C
sh-NC
sh-GINS2
PI3K
p-PI3K(Tyr458)
AKT
p-AKT(Ser473)
mTOR
p-mTOR(Ser2448)
β-actin
97H
LM3
D
oe-NC
oe-GINS2
Ly294002(20μmol/L)
HUH7
E
GINS2 mRNA
GINS2
PI3K
AKT
mTOR
GINS2 DNA
promoter
E2F1
Nucleus
Cytoplasm
Proliferation
Migration Invasion
Metastasis
Tumor progression and poor prognosis

Figure 11. GINS2 promotes HCC cell proliferation, migration, and invasion by regulating the PI3K/AKT/mTOR signaling pathway. A. Correlation between HALLMARK_PI3K_AKT_MTOR_SIGNALING and GINS2 in LIHC according to data from the TCGA database. B. Correlation between HALLMARK_PI3K_AKT_MTOR_SIGNALING and GINS2 in pan-cancers according to data from the TCGA database. C. Expression levels of PI3K/p-PI3K (Tyr458), AKT/p-AKT (Ser473), and mTOR/p-mTOR (Ser2448) in 97H and LM3 cells transfected with sh-NC or sh-GINS2 were examined by western blot. D. HUH7 cells transfected with pcDNA3.1 or pcDNA3.1-GINS2 were treated with or without the indicated concentrations of Ly294002. Expression levels of PI3K/p-PI3K (Tyr458), AKT/p-AKT (Ser473), and mTOR/p-mTOR (Ser2448) were examined by western blot. E. The model of the E2F1/GINS2 axis mediating aggressive behaviors in HCC through activating the PI3K/AKT/mTOR signaling pathway.

phorylated PI3K (Tyr458), AKT (Ser473), and mTOR (Ser2448). Conversely, a significant increase in the phosphorylation of these proteins was observed in GINS2-overexpression cells (**Figure 11C** and **11D**). However, no change of PI3K, AKT, and mTOR was observed in 97H and LM3 cells. Addition of the PI3K inhibitor Ly294002 could partially reverse the altered protein levels caused by overexpressing GINS2 (**Figure 11D**). In summary, our findings support the notion that GINS2 could promote HCC progression through the PI3K/AKT/mTOR pathway.

Discussion

Despite remarkable advances in the technology of detection and treatment, hepatocellular carcinoma (HCC) is still one of the most common and deadliest malignancies worldwide [6, 25]. Most HCC cases are diagnosed at an advanced stage and thus miss the best time window for surgery [26]. Hence, the identification of early detection biomarkers is crucial for the improvement of long-term survival of HCC patients. Various articles have reported that GINS2, as a novel oncogene, was upregulated in several malignant tumors, including breast cancer, lung cancer, pancreatic cancer, and thyroid cancer [12, 27-29]. However, the biological significance and precise mechanism of GINS2 in HCC remain to be fully elucidated.

In our research, we first assessed the possibility of GINS2 as a HCC biomarker through a series of bioinformatic analyses. The results revealed that GINS2 was aberrantly high in HCC tissues in comparison with normal ones. Kaplan-Meier curves also illustrated that higher GINS2 expression correlated with poorer OS, PFS, DSS, and RFS of HCC patients (**Figure 1**). Multivariate regression analysis similarly illustrated that GINS2 was an independent prognostic marker for HCC patients, highlighting its potential as a novel biomarker (**Figure 3**). Recent research has indicated the importance of immune cell infiltration in HCC occurrence and development [20, 22]. Besides, we found that GINS2 expression was closely involved in the infiltration of B cells, CD8+ T cells, macrophages, and dendritic cells, which indicated the importance of GINS2 in regulating HCC tumor immunity (**Figure 4**).

Functional experiments showed that the inhibition of GINS2 suppressed the proliferative, migratory, and invasive capabilities of HCC cells (**Figures 7-9**). Transcription factors (TFs) are DNA-binding proteins that activate (and less frequently, inhibit) gene transcription [30]. Therefore, we speculated that the expression of GINS2 may be regulated by TFs. The hTFtarget database was then employed for the prediction of TFs that might regulate GINS2 expression. Additionally, the results of ChIP-qPCR and dual-luciferase reporter assays uncovered that E2F1 could bind to the promoter region of GINS2 and up-regulate its expression (**Figure 10**). Numerous studies have demonstrated the transcription factor E2F1 was involved in regulating cell cycle, apoptosis, metabolism, and metastasis [31, 32]. Here, our study indicated that aberrant activation of E2F1 might upregulate the transcription of GINS2 and promote HCC progression.

The PI3K/AKT/mTOR pathway plays a crucial role in tumorigenesis [33-35]. An early study has established that KIF11 could regulate cell proliferative ability via the PI3K/AKT pathway in gallbladder cancer [36]. Another finding showed that Mex3a promotes lung adenocarcinoma metastasis via the PI3K/AKT pathway [37]. Our previous study also demonstrated that STK39 could promote the development of cholangiocarcinoma via the PI3K/AKT pathway [38]. Here, our data have added additional support to the notion that GINS2 can participate in regulating the PI3K/AKT/mTOR pathway. Knockdown of GINS2 suppressed the PI3K/AKT/

mTOR pathway and vice versa. Additionally, we found that the effect of GINS2 overexpression on PI3K/AKT/mTOR signaling could be rescued with the PI3K inhibitor LY294002.

Conclusions

Collectively, increased GINS2 expression resulted in poorer outcome of HCC patients. And further experiments revealed that GINS2 could promote HCC cell proliferative, migratory, and invasive abilities by activating the PI3K/AKT/mTOR signaling pathway. Our experiments provide important preliminary evidence that GINS2 could be a promising therapeutic biomarker for HCC. Further experiments are required to elucidate the mechanism of action of GINS2 in HCC progression.

Acknowledgements

This work was supported by grants from the National Natural Science Foundation of China (81972768 and 81870488) and the Major Program of the National Natural Science Foundation of China (81530048 and 31930020).

Disclosure of conflict of interest

None.

Address correspondence to: Xuehao Wang, Hepatobiliary Center, The First Affiliated Hospital of Nanjing Medical University, Key Laboratory of Liver Transplantation, Chinese Academy of Medical Sciences, Nanjing, Jiangsu, China. E-mail: wangxh@njmu.edu.cn; Jindao Wu, State Key Laboratory of Reproductive Medicine, Nanjing Medical University, Nanjing 210029, Jiangsu, China. E-mail: wujindao@njmu.edu.cn

References

[1] Vyas M and Zhang X. Hepatocellular carcinoma: role of pathology in the era of precision medicine. Clin Liver Dis 2020; 24: 591-610.

[2] Maluccio M and Covey A. Recent progress in understanding, diagnosing, and treating hepatocellular carcinoma. CA Cancer J Clin 2012; 62: 394-399.

[3] Lencioni R, Chen XP, Dagher L and Venook AP. Treatment of intermediate/advanced hepatocellular carcinoma in the clinic: how can outcomes be improved? Oncologist 2010; 15 Suppl 4: 42-52.

[4] Rimola J, Forner A, Tremosini S, Reig M, Vilana R, Bianchi L, Rodriguez-Lope C, Sole M, Ayuso C and Bruix J. Non-invasive diagnosis of hepatocellular carcinoma </= 2 cm in cirrhosis. Diagnostic accuracy assessing fat, capsule and signal intensity at dynamic MRI. J Hepatol 2012; 56: 1317-1323.

[5] Akamatsu N, Cillo U, Cucchetti A, Donadon M, Pinna AD, Torzilli G and Kokudo N. Surgery and hepatocellular carcinoma. Liver Cancer 2016; 6: 44-50.

[6] Bray F, Ferlay J, Soerjomataram I, Siegel RL, Torre LA and Jemal A. Global cancer statistics 2018: GLOBOCAN estimates of incidence and mortality worldwide for 36 cancers in 185 countries. CA Cancer J Clin 2018; 68: 394-424.

[7] Chang YP, Wang G, Bermudez V, Hurwitz J and Chen XS. Crystal structure of the GINS complex and functional insights into its role in DNA replication. Proc Natl Acad Sci U S A 2007; 104: 12685-12690.

[8] Carroni M, De March M, Medagli B, Krastanova I, Taylor IA, Amenitsch H, Araki H, Pisani FM, Patwardhan A and Onesti S. New insights into the GINS complex explain the controversy between existing structural models. Sci Rep 2017; 7: 40188.

[9] Gambus A, Jones RC, Sanchez-Diaz A, Kanemaki M, van Deursen F, Edmondson RD and Labib K. GINS maintains association of Cdc45 with MCM in replisome progression complexes at eukaryotic DNA replication forks. Nat Cell Biol 2006; 8: 358-366.

[10] Zhang X, Zhong L, Liu BZ, Gao YJ, Gao YM and Hu XX. Effect of GINS2 on proliferation and apoptosis in leukemic cell line. Int J Med Sci 2013; 10: 1795-1804.

[11] MacNeill SA. Structure and function of the GINS complex, a key component of the eukaryotic replisome. Biochem J 2010; 425: 489-500.

[12] Huang L, Chen S, Fan H, Ji D, Chen C and Sheng W. GINS2 promotes EMT in pancreatic cancer via specifically stimulating ERK/MAPK signaling. Cancer Gene Ther 2021; 28: 839-849.

[13] Liu X, Sun L, Zhang S, Zhang S and Li W. GINS2 facilitates epithelial-to-mesenchymal transition in non-small-cell lung cancer through modulating PI3K/Akt and MEK/ERK signaling. J Cell Physiol 2020; 235: 7747-7756.

[14] Shen YL, Li HZ, Hu YW, Zheng L and Wang Q. Loss of GINS2 inhibits cell proliferation and tumorigenesis in human gliomas. CNS Neurosci Ther 2019; 25: 273-287.

[15] Lian YF, Li SS, Huang YL, Wei H, Chen DM, Wang JL and Huang YH. Up-regulated and interrelated expressions of GINS subunits predict poor prognosis in hepatocellular carcinoma. Biosci Rep 2018; 38: BSR20181178.

[16] Wu C, Zhou Y, Wang M, Dai G, Liu X, Lai L and Tang S. Bioinformatics analysis explores potential hub genes in nonalcoholic fatty liver disease. Front Genet 2021; 12: 772487.
[17] Zhang D, Liu J, Xie T, Jiang Q, Ding L, Zhu J and Ye Q. Oleate acid-stimulated HMMR expression by CEBPalpha is associated with nonalcoholic steatohepatitis and hepatocellular carcinoma. Int J Biol Sci 2020; 16: 2812-2827.
[18] Lian Q, Wang S, Zhang G, Wang D, Luo G, Tang J, Chen L and Gu J. HCCDB: a database of hepatocellular carcinoma expression atlas. Genomics Proteomics Bioinformatics 2018; 16: 269-275.
[19] Bartha A and Gyorffy B. TNMplot.com: a web tool for the comparison of gene expression in normal, tumor and metastatic tissues. Int J Mol Sci 2021; 22: 2622.
[20] Chen S, Cao Q, Wen W and Wang H. Targeted therapy for hepatocellular carcinoma: challenges and opportunities. Cancer Lett 2019; 460: 1-9.
[21] Xu F, Jin T, Zhu Y and Dai C. Immune checkpoint therapy in liver cancer. J Exp Clin Cancer Res 2018; 37: 110.
[22] Prieto J, Melero I and Sangro B. Immunological landscape and immunotherapy of hepatocellular carcinoma. Nat Rev Gastroenterol Hepatol 2015; 12: 681-700.
[23] Vaquerizas JM, Kummerfeld SK, Teichmann SA and Luscombe NM. A census of human transcription factors: function, expression and evolution. Nat Rev Genet 2009; 10: 252-263.
[24] Brouwer I and Lenstra TL. Visualizing transcription: key to understanding gene expression dynamics. Curr Opin Chem Biol 2019; 51: 122-129.
[25] Reghupaty SC and Sarkar D. Current status of gene therapy in hepatocellular carcinoma. Cancers (Basel) 2019; 11: 1265.
[26] Forner A, Reig M and Bruix J. Hepatocellular carcinoma. Lancet 2018; 391: 1301-1314.
[27] Sun D, Zong Y, Cheng J, Li Z, Xing L and Yu J. GINS2 attenuates the development of lung cancer by inhibiting the STAT signaling pathway. J Cancer 2021; 12: 99-110.
[28] Yu S, Zhu L, Xie P, Jiang S, Wang K, Liu Y, He J and Ren Y. Mining the prognostic significance of the GINS2 gene in human breast cancer using bioinformatics analysis. Oncol Lett 2020; 20: 1300-1310.
[29] Ye Y, Song YN, He SF, Zhuang JH, Wang GY and Xia W. GINS2 promotes cell proliferation and inhibits cell apoptosis in thyroid cancer by regulating CITED2 and LOXL2. Cancer Gene Ther 2019; 26: 103-113.
[30] Pennacchio LA, Bickmore W, Dean A, Nobrega MA and Bejerano G. Enhancers: five essential questions. Nat Rev Genet 2013; 14: 288-295.
[31] Chun JN, Cho M, Park S, So I and Jeon JH. The conflicting role of E2F1 in prostate cancer: a matter of cell context or interpretational flexibility? Biochim Biophys Acta Rev Cancer 2020; 1873: 188336.
[32] Tian W, Cui F and Esteban MA. E2F1 in renal cancer: Mr Hyde disguised as Dr Jekyll? J Pathol 2013; 231: 143-146.
[33] Lien EC, Dibble CC and Toker A. PI3K signaling in cancer: beyond AKT. Curr Opin Cell Biol 2017; 45: 62-71.
[34] Bertacchini J, Heidari N, Mediani L, Capitani S, Shahjahani M, Ahmadzadeh A and Saki N. Targeting PI3K/AKT/mTOR network for treatment of leukemia. Cell Mol Life Sci 2015; 72: 2337-2347.
[35] Wu Y, Zhang Y, Qin X, Geng H, Zuo D and Zhao Q. PI3K/AKT/mTOR pathway-related long noncoding RNAs: roles and mechanisms in hepatocellular carcinoma. Pharmacol Res 2020; 160: 105195.
[36] Wei D, Rui B, Qingquan F, Chen C, Ping HY, Xiaoling S, Hao W and Jun G. KIF11 promotes cell proliferation via ERBB2/PI3K/AKT signaling pathway in gallbladder cancer. Int J Biol Sci 2021; 17: 514-526.
[37] Liang J, Li H, Han J, Jiang J, Wang J, Li Y, Feng Z, Zhao R, Sun Z, Lv B and Tian H. Mex3a interacts with LAMA2 to promote lung adenocarcinoma metastasis via PI3K/AKT pathway. Cell Death Dis 2020; 11: 614.
[38] Hao X, Zhang Y, Lu Y, Han G, Rong D, Sun G, Sun G, Tang W, Wu J and Wang X. STK39 enhances the progression of Cholangiocarcinoma via PI3K/AKT pathway. iScience 2021; 24: 103223.

Table S1. Primer sequences used for real-time PCR (5' to 3')

Symbol	Primer	Sequence (5'→3')
GINS2	Forward Primer	CCCTGGTTTACCCGTGGAAG
	Reverse Primer	GGGAGCAGGCGACATTTCT
E2F1	Forward Primer	CATCAGTACCTGGCCGAGAG
	Reverse Primer	CCCGGGGATTTCACACCTTT
GAPDH	Forward Primer	TCGACAGTCAGCCGCATCTT
	Reverse Primer	AGGCGCCCAATACGACCAAA
β-actin	Forward Primer	AGCGAGCATCCCCCAAAGTT
	Reverse Primer	GGGCACGAAGGCTCATCATT

Table S2. Information of antibodies used in present study

Antibody	Catalog	Specificity	Company
E2F1	66515-1-Ig	Mouse monoclonal	Proteintech, China
GINS2	ab197123	Rabbit, polyclonal	Abcam, USA
PI3K	4292	Rabbit, polyclonal	CST, USA
p-PI3K	4228	Rabbit, polyclonal	CST, USA
AKT	9272	Rabbit, polyclonal	CST, USA
p-AKT	9271	Rabbit, polyclonal	CST, USA
mTOR	2972	Rabbit, polyclonal	CST, USA
p-mTOR	2971	Rabbit, polyclonal	CST, USA
CDK2	22060-AP	Rabbit, polyclonal	Proteintech, China
CDK4	11026-1-AP	Rabbit, polyclonal	Proteintech, China
CCND1	60186-1-Ig	Mouse monoclonal	Proteintech, China
VEGF	19003-1-AP	Rabbit, polyclonal	Proteintech, China
Ki-67	ab15580	Rabbit, polyclonal	Abcam, USA
β-actin	ab8227	Rabbit, polyclonal	Abcam, USA

Table S3. Sequence of primers for ChIP assay

GINS2-chip-primer	Sequence (5' to 3')
GINS2-E1-left	GGCTGTCTACCGCCTTCCTATAG
GINS2-E1-right	CAGAGCCTCACGGTCTCCTCG
GINS2-E2-left	CCCCACCCCCGGCTCTTGATTAGG
GINS2-E2-right	GGCGTGCACCTGGCGCTGTCAG
GINS2-E2-right	GGCGTGCACCTGGCGCTGTCAG
GINS2-E3-right	ATTCGGACACTTCAGAGCAGGAG

Table S4. GINS2 expression associated with clinical pathological characteristics (logistic regression)

Characteristics	Total (N)	Odds Ratio (OR)	*P* value
T stage (T2 & T3 & T4 vs. T1)	368	2.019 (1.336-3.067)	< 0.001
N stage (N1 vs. N0)	256	0.924 (0.109-7.795)	0.937
M stage (M1 vs. M0)	270	0.305 (0.015-2.413)	0.306
Pathologic stage (Stage III & Stage IV vs. Stage I & Stage II)	347	1.739 (1.072-2.850)	0.026
Tumor status (With tumor vs. Tumor free)	352	1.758 (1.149-2.701)	0.010
Histologic grade (G3 & G4 vs. G1 & G2)	366	2.710 (1.750-4.241)	< 0.001
Vascular invasion (Yes vs. No)	315	1.352 (0.849-2.159)	0.204

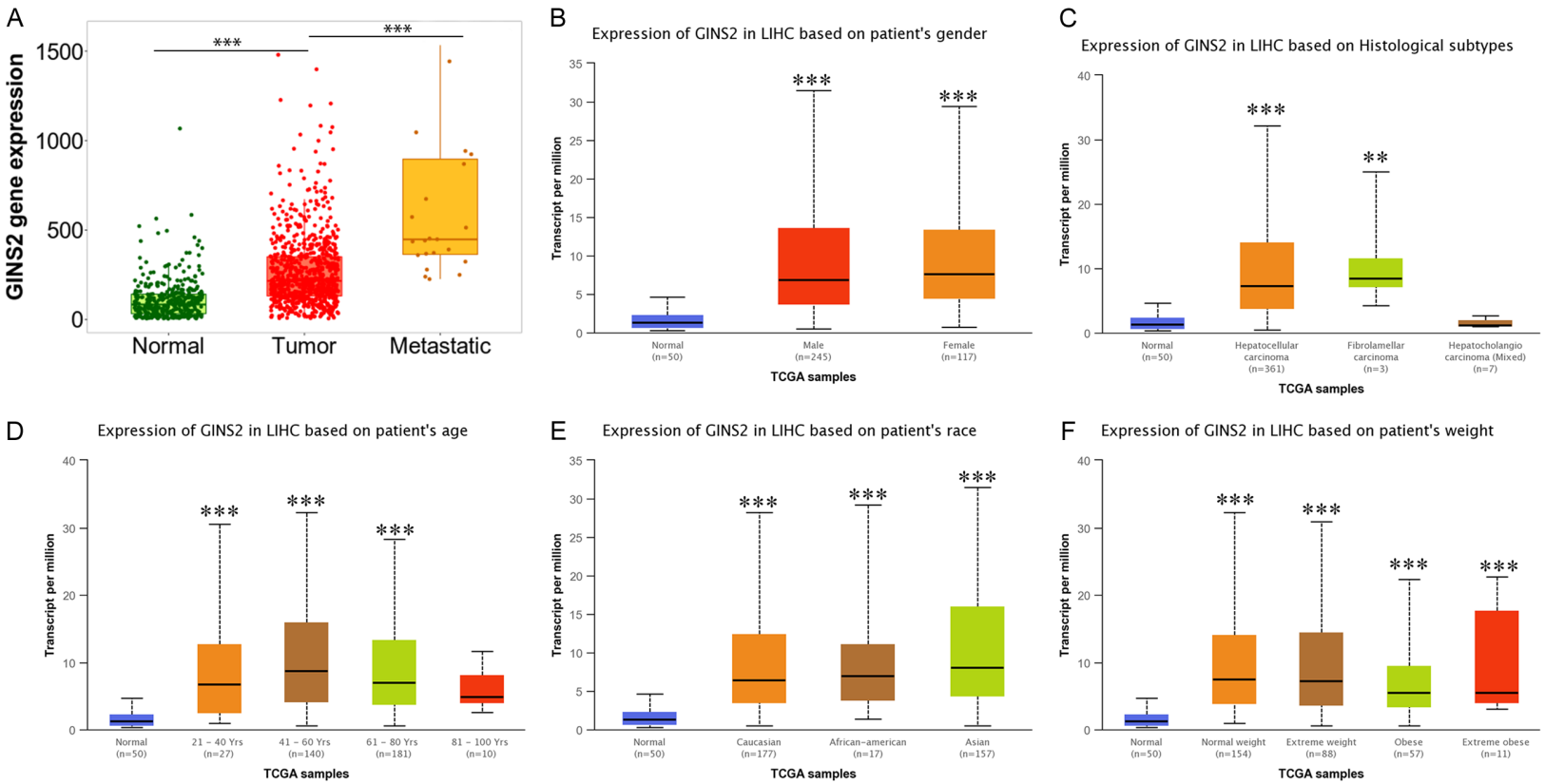

Figure S1. Box plot evaluating GINS2 expression in subgroups of LIHC samples (UALCAN and TNMplot). Upregulated mRNA of GINS2 is independent of patients' metastatic status (A), gender (B), histological subtypes (C), age (D), race (E), and weight (F). The t-test was used to estimate the significance of differences in gene expression levels between groups. *P < 0.05; **P < 0.01; ***P < 0.001.

Table S5. Univariate and multivariate Cox's regression analysis of factors associated with OS in HCC

Characteristics	Total (N)	Univariate analysis		Multivariate analysis	
		Hazard ratio (95% CI)	*P* value	Hazard ratio (95% CI)	*P* value
Age	370				
≤ 60	177	Reference			
> 60	193	1.248 (0.880-1.768)	0.214		
Gender	370				
Male	249	Reference			
Female	121	1.225 (0.860-1.746)	0.260		
Pathologic stage	346				
Stage I & Stage II	256	Reference			
Stage III & Stage IV	90	2.449 (1.689-3.549)	< 0.001	1.527 (0.208-11.194)	0.677
T stage	367				
T1 & T2	274	Reference			
T3 & T4	93	2.540 (1.785-3.613)	< 0.001	1.410 (0.192-10.359)	0.736
N stage	256				
N0	252	Reference			
N1	4	2.004 (0.491-8.181)	0.333		
M stage	270				
M0	266	Reference			
M1	4	4.032 (1.267-12.831)	0.018	1.870 (0.423-8.273)	0.409
Tumor status	351				
Tumor free	201	Reference			
With tumor	150	2.361 (1.620-3.441)	< 0.001	1.960 (1.226-3.133)	0.005
Histologic grade	365				
G1 & G2	232	Reference			
G3 & G4	133	1.120 (0.781-1.606)	0.539		
Vascular invasion	314				
No	206	Reference			
Yes	108	1.348 (0.890-2.042)	0.159		
AFP (ng/ml)	277				
≤ 400	213	Reference			
> 400	64	1.056 (0.646-1.727)	0.827		
GINS2	370				
Low	185	Reference			
High	185	1.692 (1.193-2.399)	0.003	1.653 (1.023-2.671)	0.040

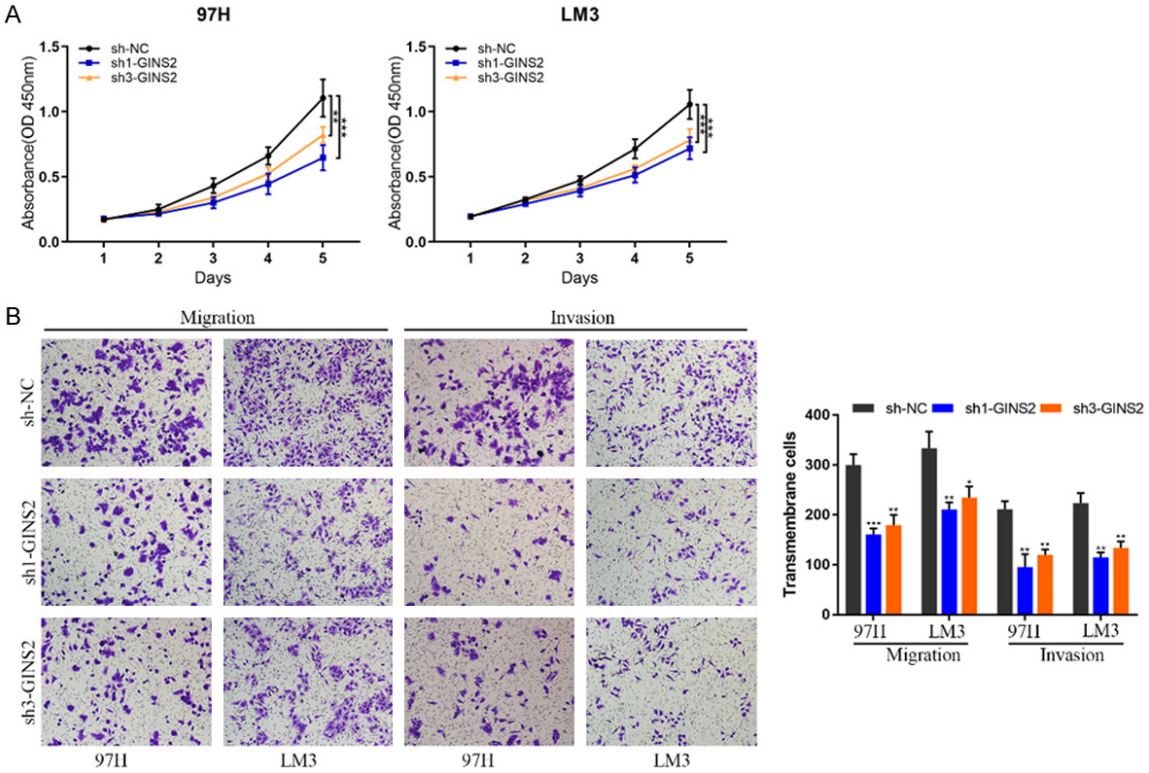

Figure S2. Knockdown of GINS2 suppresses cell proliferation, invasion, and migration of HCC cells *in vitro*. A. CCK-8 assay was performed in 97H and LM3 cells transfected with sh-NC, sh1-GINS2, or sh3-GINS2. B. Invasive or migrated cells were measured by transwell assay with or without matrigel. All data are represented as the means ± S.E.M. *P < 0.05; **P < 0.01; ***P < 0.001.

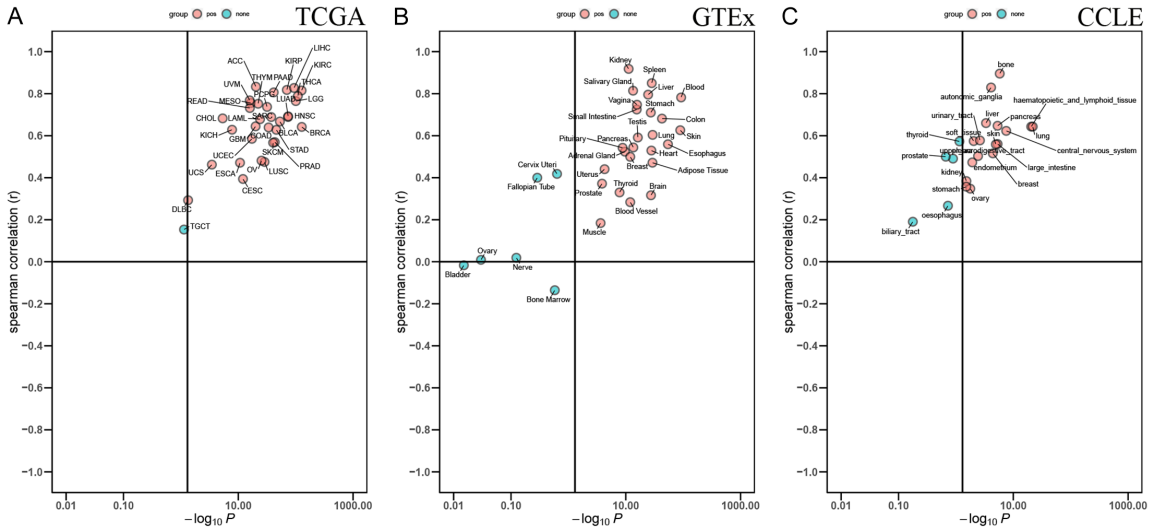

Figure S3. Correlation analysis of E2F1 and GINS2. The expression levels of E2F1 and GINS2 showed a strong positive correlation in the TCGA (A), GTEx (B), and CCLE (C) databases.

A

Matrix ID	Name	Score	Relative score	Sequence ID	Start	End	Strand	Predicted sequence
MA0024.2	MA0024.2.E2F1	12.949903	0.96284942074905	NC_000016.10:c85690954-85688855	1967	1977	+	GTGGCGGGAAA
MA0024.2	MA0024.2.E2F1	12.097759	0.9500291553819264	NC_000016.10:c85690954-85688855	1716	1726	-	CGGGCGCCAGC
MA0024.2	MA0024.2.E2F1	11.742697	0.9446873362979559	NC_000016.10:c85690954-85688855	1186	1196	-	GGAGCGGCAGG

B

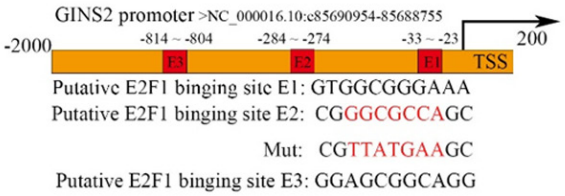

Figure S4. Potential E2F1 binding sequences on the GINS2 promoter regions. A. Three E2F1 binding sequences on the GINS2 promoter regions according to the JASPAR website. B. Mutant sequences used in the dual-luciferase reporter assay.